COMPUTATIONAL MODELLING OF FREE SURFACE FLOW IN INTAKE
STRUCTURES USING FLOW 3D SOFTWARE

A THESIS SUBMITTED TO
THE GRADUATE SCHOOL OF NATURAL AND APPLIED SCIENCES OF
MIDDLE EAST TECHNICAL UNIVERSITY

BY

AKIN AYBAR

IN PARTIAL FULFILLMENT OF THE REQUIREMENTS
FOR
THE DEGREE OF MASTER OF SCIENCE
IN
CIVIL ENGINEERING

JUNE 2012

Approval of the thesis:

COMPUTATIONAL MODELLING OF FREE SURFACE FLOW IN INTAKE STRUCTURES USING FLOW 3D SOFTWARE

submitted by **AKIN AYBAR** in partial fullfillment of the requirements for the degree of **Master of Science in Civil Engineering Department, Middle East Technical University** by,

Prof. Dr. Canan Özgen   _____
Dean, Graduate School of **Natural and Applied Sciences**

Prof. Dr. Güney Özcebe   _____
Head of Department, **Civil Engineering**

Prof. Dr. İsmail Aydın   _____
Supervisor, **Civil Engineering Dept., METU**

Examining Comittee Members:

Prof. Dr. Mustafa Göğüş   _____
Civil Engineering Dept., METU

Prof. Dr. İsmail Aydın   _____
Civil Engineering Dept., METU

Assoc. Prof. Dr. Zafer Bozkuş   _____
Civil Engineering Dept., METU

Assist. Prof. Dr. Mete Köken   _____
Civil Engineering Dept., METU

Assist. Prof. Dr. Ender Demirel   _____
Civil Engineering Dept., ESOGU

Date: June 18, 2012

I hereby declare that all information in this document has been obtained and presented in accordance with academic rules and ethical conduct. I also declare that, as required by these rules and conduct, I have fully cited and referenced all material and results that are not original to this work.

Name, Last Name : Akın Aybar

Signature   :

ABSTRACT

COMPUTATIONAL MODELLING OF FREE SURFACE FLOW IN INTAKE STRUCTURES USING FLOW 3D SOFTWARE

AYBAR, Akın

M.Sc., Department of Civil Engineering

Supervisor: Prof. Dr. Ismail AYDIN

June 2012, 64 Pages

Intakes are inlet structures where fluid is accelerated to a certain flow velocity to provide required amount of water into a hydraulic system. Intake size and geometry affects the formation of flow patterns, which can be influential for hydraulic performance of the whole system. An experimental study is conducted by measuring velocity field in the hydraulic model of the head pond of a hydropower plant to investigate vortex formation. Vortex strength based on potential flow theory is calculated from the measured velocity field. It was shown that vortex strength increases with the submergence Froude number. The free surface flow in the head pond is simulated using Flow-3D software. Vortex strength calculations are repeated using the computational velocity distributions and compared to experimentally obtained values. Similar computations were carried on with some idealized pond geometries such as rectangular and circular.

Keywords: Intake vortices, Vortex formation, Vortex strength, Intake submergence

ÖZ

SUALMA YAPILARINDAKİ SERBEST YÜZEYLİ AKIMLARIN FLOW-3D YAZILIMIYLA SAYISAL OLARAK MODELLENMESİ

AYBAR, Akın

Yüksek Lisans, İnşaat Mühendisliği Bölümü

Tez Yöneticisi: Prof. Dr. İsmail AYDIN

Haziran 2012, 64 Sayfa

Sualma yapıları, yeterli miktarda suyu hidrolik sistem içine çekmek için suyun belirli bir hıza ulaştırıldığı giriş yapılarıdır. Sualma yapısının büyüklüğü ve şekli tüm sistemin başarımını etkileyen akım düzenlerinin oluşmasında belirleyicidir. Bir hidroelektrik santralin yükleme havuzunun hidrolik modelinde hız alanları ölçülerek vorteks oluşumu incelenmesine yönelik bir deneysel çalışma gerçekleştirilmiştir. Potansiyel akım teorisine dayandırılarak, ölçülen hız dağılımlarından vorteks dayanımları hesaplanmıştır. Vorteks dayanımının batıklık Froude sayısı ile arttığı gösterilmiştir. Yükleme havuzu içindeki serbest yüzeyli akımın Flow 3D yazılımı ile sayısal çözümü yapılmıştır. Vorteks dayanım hesapları sayısal çözümden bulunan hızlar kullanılarak tekrarlanmış ve ölçümlerden elde edilen değerlerle karşılaştırılmıştır. Benzer hesaplamalar dikdörtgen ve daire gibi ideal şekilli yükleme havuzları için de gerçekleştirilmiştir.

Anahtar Kelimeler: Sualma yapısı vorteksleri, Vorteks oluşumu, Vorteks dayanımı, Sualma yapısı batıklığı

ACKNOWLEDGMENTS

TABLE OF CONTENTS

LIST OF TABLES

TABLES

LIST OF FIGURES

FIGURES

LIST OF SYMBOLS

C_D Coefficient of discharge

d Intake diameter (m)

F_R Submergence Froude number

g Acceleration due to gravity (m/s^2)

s/d Dimensionless intake submergence

K Vortex Strength (m^2/s)

k Turbulent kinetic energy (m^2/s^2)

N_Γ Circulation number

P Pressure (N/m^2)

q Specific discharge (m^2/s)

Q Intake discharge (m^3/s)

r General radius (m)

R_R Radial Reynolds number

s Intake submergence (m)

s_{cr} Critical submergence (m)

U_{avg} Average velocity in the conveyance tunnel exit (m)

U_∞ Uniform canal velocity (m/s)

$U\tau$ Shear velocity

y   Distance to the wall boundary (m)

y^+ Dimensionless distance to the wall boundary

y_1^+ Dimensionless distance from center of the adjacent cell to the wall boundary

V   Intake velocity (m/s)

V_t Tangential velocity (m/s)

W_e Weber number

z   Elevation (m)

ν Kinematic viscosity (m^2/s)

ϕ Potential function

θ Angular variable

ε Eddy viscosity

Γ Circulation

CHAPTER 1

INTRODUCTION

1.1. Intake Vortices

In modern world, electricity production and water demand are arguably two most critical issues of humanity. Collecting water in reservoirs and using for energy production is an effective way to deal with both problems. Collection of water for energy is managed by intakes in reservoirs. As in all engineering projects, designing of the intakes are handled by two principles; minimizing the cost and maximizing the efficiency. Design criteria and economical restrictions may force the designer to end up with intake designs that display undesirable flow conditions, such as vortex. Vortices may be formed due to several reasons, however three main categories were pointed out by Durgin & Hecker (1978) (Guidelines for Design of Intakes For Hydraulic Plants, 1995). The categories are:

a) Eccentric orientation of the intake
b) Viscous induced velocity gradients
c) Formations of eddies by obstructions
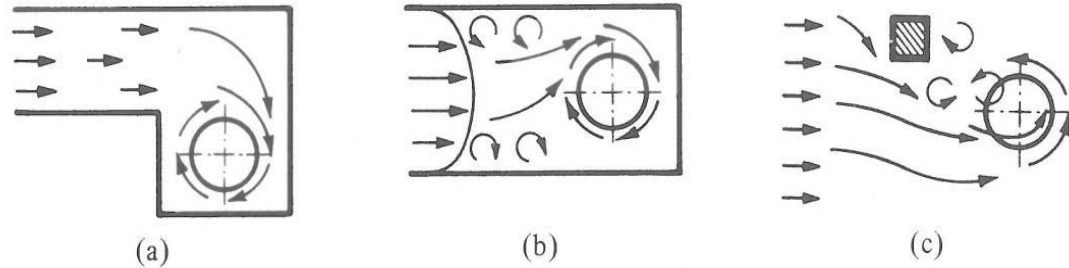
Figure 1.1 Causes of vortices (Durgin & Hecker 1978)

Vortices can both take place in pump sumps and power intake structures. Features of intakes gain importance when vortex formation is considered. A subclassification was proposed by Knauss (1987), defining intake types by two consideration points; namely orientation and location of the intake. Orientation of the intake is about the direction and alignment of the intake, which was subcategorized as vertically downwards, inclined downwards, horizontal, inclined upwards and vertically upwards. Second consideration point is the intake location, whether the intake is located on a wall or projected into the pool area.

Vortices are also classified among themselves, since their presence in intakes may be tolerable to a certain extent. A qualitative classification was made, since it is impossible to set a quantitave criteria. Although subjective, evaluation of vortices' strength proved to be helpful for intake designs. Categories for vortex strength were created at Alden Research Laboratory (Knauss, 1987). The strength categories can be listed as follows:

a) Very weak eddies without observable depression in flow area.
b) Coherent swirl at surface with visible, small depression.
c) Vortex formation through the intake, visible only when dye introduced to the flow region.
d) Vortex within limits that does not take air into the intake, however pulls debris

e) Vortex formation with air introduction through the intake, however process is intermittent

f) Fully developed air core vortex

Vortex formation that are not tolerable creates undesired results for intakes; namely high head losses, air introduction that causes cavitation and vibration in the system, increased wearing rate in used material, decreased flow efficiency and debris entrance through the intake. Vortices may occur both at the surface and in subsurface level. While surface vortices creating disadvantage of suction of air and debris, subsurface vortices create swirl intrusion in intakes or pump sumps. Both type of vortices can be investigated in terms of steadiness. Instability in surface vortices can be determined by air suction and swirl continuity. For subsurface vortices, swirl intrusion should be detected and the the vortex should start from the floor or the walls of the upstream basin.

Prevention method in intakes can be listed as increasing submergence, improving the approach flow conditions and building anti vortex devices. Among all solutions, increasing submergence to supress the vortex formation is the most practiced one. Submergence can be defined as the elevation difference between bottom level of the intake and the free surface elevation. To deliver a proper design of intake, critical submergence value should be known. Critical submergence is the level of submergence that is just before the vortex formation starts. Checks for the critical submergence in intakes are mainly conducted by using formulae proposed by scientists, however it is difficult to determine exact critical submergence levels, since every intake structure have unique conditions and the formulae are based on empirical studies.

VORTEX
TYPE (VT)

1   COHERENT SURFACE SWIRL

2   SURFACE DIMPLE;
COHERENT SWIRL AT SURFACE

3   DYE CORE TO INTAKE;
COHERENT SWIRL THROUGHOUT
WATER COLUMN

4   TRASH   VORTEX PULLING FLOATING
TRASH, BUT NOT AIR

5   AIR BUBBLES   VORTEX PULLING AIR
BUBBLES TO INTAKE

6   FULL AIR CORE
TO INTAKE
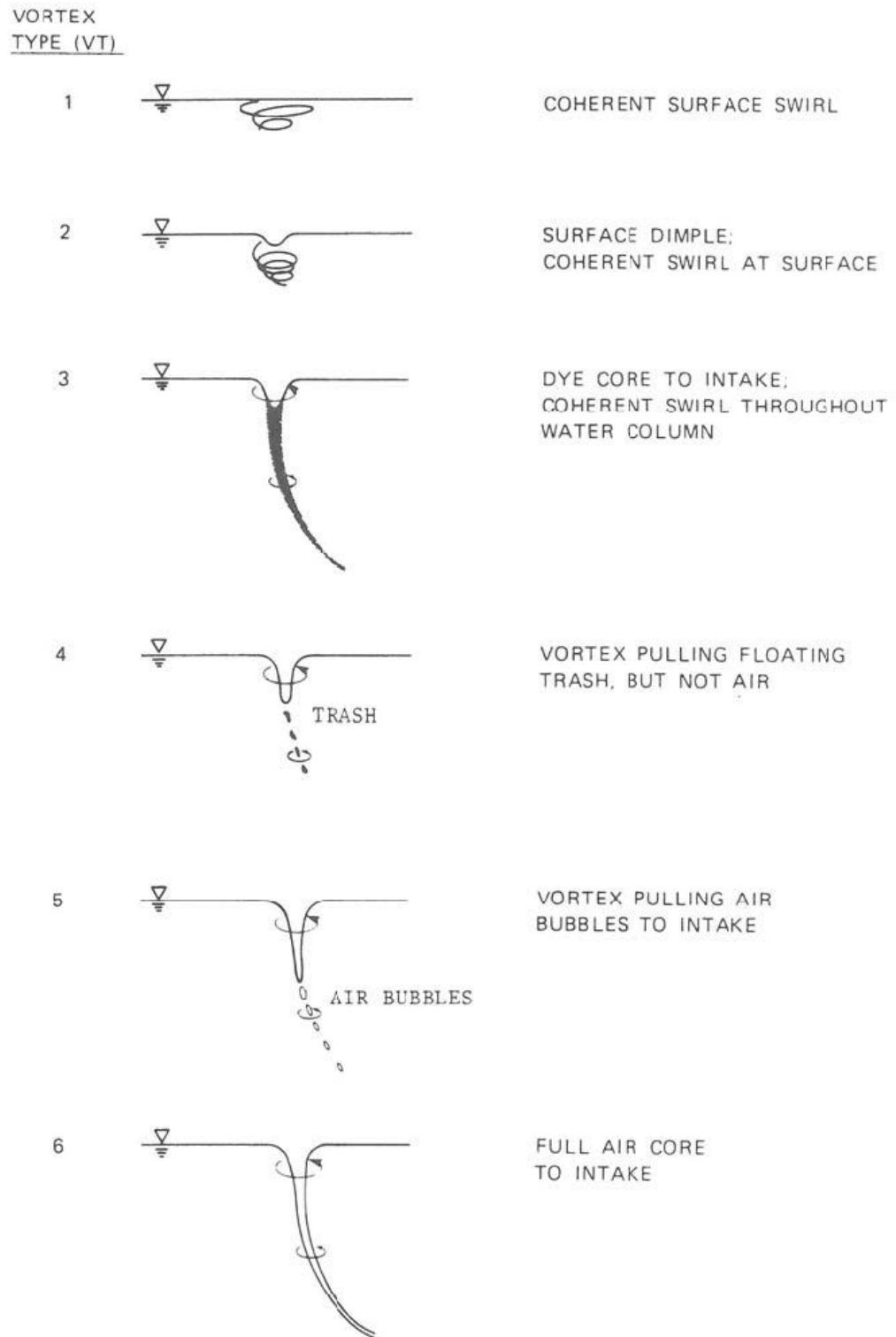
Figure 1.2 ARL vortex type classification (Knauss, 1987)

4

Unwanted flow conditions in intakes are mostly observed and studied by constructing scaled models. Computational fluid dynamics (CFD) concepts are available now for scientists to validate these formulae, thanks to the the recent developments in the computers' capability. Comparison of CFD results with those of actual models has been made in recent years. Although earlier studies had not attained success, recent studies have shown that numerical models may achieve adequate precision and accuracy.

1.2. Literature Survey

Many studies are available with both analytical and numerical solutions, when problems at intakes are considered. In recent studies, investigation of vortices with computational fluid dynamics software has also been practiced. Investigations have been conducted in both numerical and physical areas. Assumptions were made to simplify the equations derived, since many factors may be affecting vortex formation. Most of the studies have been based on physical studies with empirical approach, due to complexity. Assumptions may divert results from actual values. Each case has its own unique conditions in terms of geometry and boundary conditions, thus constructing physical models is preferred for vortex investigation. Navier-Stokes equations has mathematical complexity to define vortex formation analytically. Thus, in analytical studies, researchers tried to simplify the determination of vortex behavior. In numerical basis, methods such as finite element method were used to simulate flow conditions.

Einstein & Li (1955) made some simplifying assumptions in Navier-Stokes equations, including radial symmetry, absence of vertical velocity, horizontal flow velocities without vertical variation, steady flow and hydrostatic pressure. Eddy viscosity concept was used, meaning that smaller turbulence effects are ignored. Consideration of turbulance was used for increasing effective flow viscosity. When the assumption of neglecting vertical variation in horizontal

directions was made, automatically, the boundary layer effect vanished from the results (Knauss, 1987).

Blaisdell (1958) proposed constructing a hood to prevent any vortex formation within the flow area (Guidelines for Design of Intakes for Hydroelectric Plants, 1995).

Lewellen (1962) pointed out that investigation of vortex formation without dependancy of system type can be achieved by using dimensionless parameters. His studies were based on vertical variations of horizontal velocities near the core, among consequences of ignoring the boundary layer and identified several dimensionless numbers relevant and important to the vortex phenomena. (Knauss, 1987).

$$F_r = V/\sqrt{gh} \qquad \text{= submergence Froude number} \qquad (1.1)$$

$$N_\Gamma = (\Gamma d)/Q \qquad \text{= circulation number} \qquad (1.2)$$

$$R_R = Q/(\nu h) \qquad \text{= radial Reynolds number} \qquad (1.3)$$

$$s/d \qquad \text{= dimensionless intake submergence} \qquad (1.4)$$

$$W_e = V\sqrt{\rho d/\sigma} \qquad \text{= Weber number} \qquad (1.5)$$

where V is the intake velocity, g is the acceleration due to gravity, h is the intake submergence, k is the circulation, d is intake diameter, Q is the intake discharge, σ is the surface tension and ν is kinematic viscosity. Holtroff (1964) derived a numerical method with the same assumptions that Einstein & Li (1955) determined, obtaining better prediction of surface depression and velocity field next to the core. (Knauss, 1987).

To determine the circulation number Γ, the following equation

$$\Gamma = 2\pi r V_t \qquad (1.6)$$

where r is the radius and V_t is the tangential velocity. The equation can be derived from Navier stokes equations, for thecase of axisymmetrical vortex flow

(Granger, 1966). In theory, k should not change with changing r value for an ideal fluid forming free vortex (Knauss, 1987).

Bottom boundary layer has impact on vortex phenomena. Studies and experiments of Anwar (1965,1966, 1967,1968) displayed that roughened bottom can dissipate potential vortices that had been present in the flow area with smoother surface. Ideal free vortex distribution was also defined in studies, except near vortex core. Approximate surface depression at the vortex center was formulated. Anwar stated that large air core in vortices would have an impact on the inlet loss coefficient. From these studies, Anwar reported that in weak vortices, shape of vortex becomes cylindrical. All measurements were taken from near air core. Studies revealed that for strong steady and narrow air core vortices, viscosity has no significant impact for $R_R > 10^3$ and scales beyond 1/20 would not be adequate to express Froude number effect (Knauss, 1987).

Gordon (1970) determined four main criteria that take role in formation of vortices in intakes: approach flow geometry to the intake, velocity at flow region, critical submergence and size of the intake. Total of 29 hydroelectric intake had been studied to derive equation for industrial usage. Two equations were proposed:

$$\left(\frac{h}{d}\right)_{cr} = 2.3 \ F_r \qquad (1.7)$$

for asymmetrical cases and

$$\left(\frac{h}{d}\right)_{cr} = 1.7 \ F_r \qquad (1.8)$$

for symmetrical cases (Knauss, 1987). Gordon's study has importance to display linear relation of critical submergence levels with Froude number. Toyokura & Akaide (1970) revealed that near the air core, the circulation decreases to zero (Knauss, 1987).

Daggett & Keulegan (1974) conduct their investigations on the viscosity effects in vortex formation, adressing limiting points. Investigations revealed that radial

velocity u in vortices varies with depth z, opposite to the theoretical analyses that du/dz = 0. Size and shape of vortex and the efficiency of flow were investigated. From the study of vortex flow through orifices, the limit to neglect viscous effect was found as

$$\frac{Q}{vs} > 2.5 * 10^4 \tag{1.9}$$

The same study showed that surface tension effects becomes negligible for We > 10^4 (Knauss, 1987). Effects of vortex formation on discharge was discussed. For Re < 10^4, viscous effects become effective, thus coefficient of discharge becomes dependent only on the Reynolds number. In the experiments, same viscosities were used, surface tension was changed from 0.072 to 0.024 N/m. However, no effect was observed on coefficient of discharge.

Prosser (1977) stated that to avoid vortex formation, channel condition has to be uniform, single phase and steady when the flow passes from free surface to channel conditions. It was proposed that required minimum submergence can be achieved if $s_{cr} \geq 2.5$ d, assumed that V = 4 m/s, 0.5 < F_r < 2 and 10^6< Re < 10^7. Recommendations were limited by small to medium installations.

Durgin & Hecker (1978) defined three types of vorticity sources (Figure 1.1). A plot was drawn with Froude number to the observed type of vortex. It was concluded that, as F_r increased, swirl in the flow region got stronger.

Brocard et al. (1982) based the investigations on proving the numerical ability of experiments by conducting finite element method for withdrawal from a reservoir. The circulation is eccentricly placed when the geometry is considered. The circulation had needed some time to be formed, due to the location of the sink in the reservoir. Flow area tried to be simulated in 2D and with 240 elements, with time step of 1.25 seconds. ε = 10 m^2/s was used farther from the outlet, where ε is the eddy viscosity. However, that value was set to 2 m^2/s near the vortex. The results have shown that numerical calculations did not reflect the actual values. It was stated that the numerical techniques were not reliable enough to use in practice (Knauss, 1987).

Padmanabhan & Hecker (1984) conducted studies on scaling effect on the free surface vortex formation in pump sumps. To conduct the investigation, two models were considered with scale of 1/2 and 1/4 as pump sumps. Studies revealed that modelling with scale of 1/2 and 1/4 creates negligable scaling effects of vortex formation. However, the comparison was conducted by making comparison in vortex type basis, not critical submergence (Figure 1.1). Thus, for critical submergence consideration, different results may be obtained. The results are also reliable for Re > 10^5 where Re = Vd/ν. For Re < 10^5, scaling effects were observed due to higher losses in ratio for the reduced scale cases, when compared to full-scale model.

Gulliver and Rindels (1987) conducted studies on weak surface vortices at vertical intakes with headrace channel by experimental models. Guide vanes were placed to set the approach angle to the headrace, thirteen experiments were conducted with different approach angles and Froude number ranges between 0.25 and 2.2. Variations of s/d with Froude number was provided.

It was also noted that, it requires serious submergence levels to suppress weak vortices, thus anti vortex devices may be required.

Hite and Mih (1994) based studies on theoretical determination of equations for axial, radial and tangential velocities. Studies were also containing water surface profile of vortices formed in the flow area. Findings were proved successful with the actual experimental observations.

Yıldırım and Kocabaş (1995) concentrated studies on critical submergence determination in intakes with air core vortex formation. Experimentally, Rankine ovoids were investigated and theoretical studies were made. To form flow area theoretically, a point sink was superposed with uniform channel flow. In this study, the discharge of the point sink was equated to the discharge of fhe uniform flow to provide continuity in the system. In this experiment, the critical submergence level was set to radius of the imaginary point sink. By both

theoretical findings and empirical studies, critical submergence was formulated as

$$\frac{h_{cr}}{d} = \frac{1}{2\sqrt{2}} (C_d \frac{V}{U_\infty})^{1/2}$$

(1.10)

where C_D is the coefficient of discharge and U_∞ is the uniform canal flow velocity. Application of the formula in the intake in Sakarya River, Turkey gave consistent results.

Rajendran et al. (1998) conducted a study to compare physical model and numerical model of a pump sump. Physical model of pump sump setup formed with complex turbulent flow properties and turbulent flow, allowing to form free surface and wall attached vortices. Setup was created in conditions that surface tension effects may be neglected. Particle image velocimetry was used to conduct measurements on the physical model, by creating visualizations with dye. Numerical models were based on Reynolds averaged Navier-Stokes equations. In the study, single free surface vortex was predicted successfully, however it was reported that the structure of the formed vortex was somewhat different from the physical case. The size of the vortex was predicted bigger in the numerical model, when compared with the physical one.
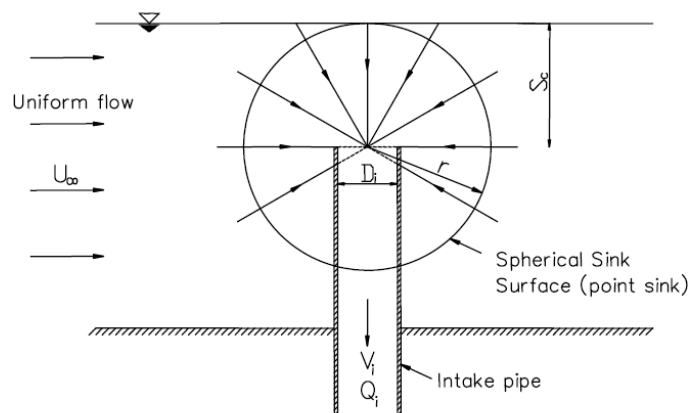
Figure 1.3 Superposition of uniform flow and point sink, in the experiment of Yıldırım & Kocabaş (1995)

(a) Numerical
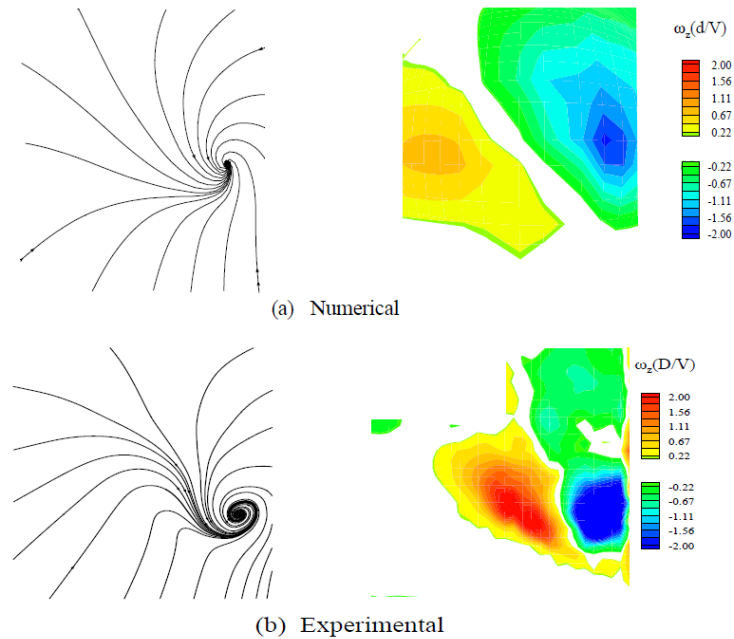
(b) Experimental

Figure 1.4 Comparison of numerical and experimental floor vortex formation in streamlines and vorticity (Rajendran et al. 1998).

Circulation strengths for the vortices were also found different, except for the vortex attached to the side wall nearer to the intake pipe. The study proposed that meandering structure of the vortices in a pump sump creates difficulty for numerical problems to simulate vortices properly. However, numerical models may be used as an auxillary tool to determine whether vortex formation may occur in a pump sump.

Yıldırım et al. (2000) considered flow boundary effects, on the critical submergence in intake pipe . A horizontal intake pipe with dead end canal flow was taken as subject. The results proved that, the distance between a dead end and the intake pipe has effects, when the data is compared with the theoretical values. As the distance decreases, different results were obtained with theoretical findings. It was suggested that potential flow method may provide better results if s_{cr} is greater than distance between the dead end and the intake pipe. The potential flow makes the assumption that the center point of the intake coincides with the point of entry of the air core vortex. The situation may change if the dead end becomes much smaller, overprediction may become a problem.

11

Yıldırım (2004) conducted investigations for the critical submergence in a rectangular intake. In the study, theoretical model setup was chosen as Rankine half body, which can be obtained by superposing line sink and uniform flow. The potential solution gave reliable results when the distance to impervious flow boundaries were not much smaller than the critical submergence. However, if the distances had been much smaller than the critical submergence, the results would have been overestimating the actual ones by 80 %.

Okamura et al. (2007) conducted numerical studies on pump sumps in numerical basis with several CFD programs, to compare with physical model. It was noted that, at physical model, required critical submergence levels were increasing nearly propotional with the flow rate in the sump. It was also mentioned that vortex formations were in the forms of air core and unsteady. Velocity and vorticity distributions were obtained by using particle image velocimetry. According to the findings, when an air core vortex was formed due to the high velocities and low submergence level, a subsurface vortex were accompanying. In the numerical area, some CFD codes proved to be successful to give outputs with adequately accurate values for industrial usage. However, distribution of magnitudes of vorticity was different from the physical case, may be caused from the lack of accuracy of the CFD computation.

1.3. Scope of the Present Study

Vortex formation in vertical intakes is a critical problem for most designers. The complex flow structure and the uniqueness of the problem for each intake structure forces designers to conduct studies on physical models. Evidently, numerical model construction for intakes saves both time and money, when compared with physical model construction. Since the capabilities of hardware and software have been increasing, the numerical models have started to became the first choice to give more reliable results. Thus, by using a commercial software, designers may study vortex formation on a software enviroment without necessity of constructing a physical model. The scope of the

study is to investigate the air core vortex formation in vertical intakes by highlighting the ability and shortcomings of the CFD code, when vortex formation and critical submergence are considered.

CHAPTER 2

HYDRAULIC MODEL STUDY

2.1. Adacami Project

Adacami Dam is located in Rize, Turkey. Feasibility study of the project and the final calculations were made by EN-SU Engineering and Consultation. Construction has been underway since 23/06/2009. Constructing firm is Taşeli Construction Trade and Industry Limited Company, employed by Çalık Energy Trade and Industry Joint Stock Company. Adacami Dam will have the installed power of 29 MW by two turbines. 26 m^3/s is the maximum discharge, 13 m^3/s is the average discharge and 4.15 m^3/s is the firm flow discharge. Tyrolean weir was chosen to collect water from three regulators (www.taseli.com.tr).

Adacami intake was designed as a vertical power intake, which has a tetragon shape with approach angle of zero. A side spillway was placed on the right hand side of the intake to allow overflow of excess water. Side spillway has the height of 2.92 meters from the intake bottom.

2.2. Hydraulic Model

The hydraulic model of the Adacami Dam's power intake was construced in the hydromechanics laboratory of Civil Engineering Department at Middle East Technical University. Similitude between the model and the prototype was

based on equality of Froude numbers. The model has the intake pipe diameter of 0.207 m, where the prototype diameter is 3.4 m. From the length ratio, model scale was found as 1/16.43. The model covers 65 meters of conveyence tunnel length, intake pool and 30 meters of the penstock length. Hydraulic model was placed over a 2 m high concrete platform with a horizontal area of 3.5 m x 4.5 m (Figure 2.1) (Figure 2.2). To observe the flow conditions, the transition to the penstock, bed and side walls of the model were formed with transparent plexi-glass. In this section, if not mentioned, all numerical values given will be valid for the model scale, since the numerical studies were conducted for the model. The design flowrate of the intake structure is 0.023 m^3/s. A strong free surface vortex was observed in the model for the design flowrate (Figure 2.3).
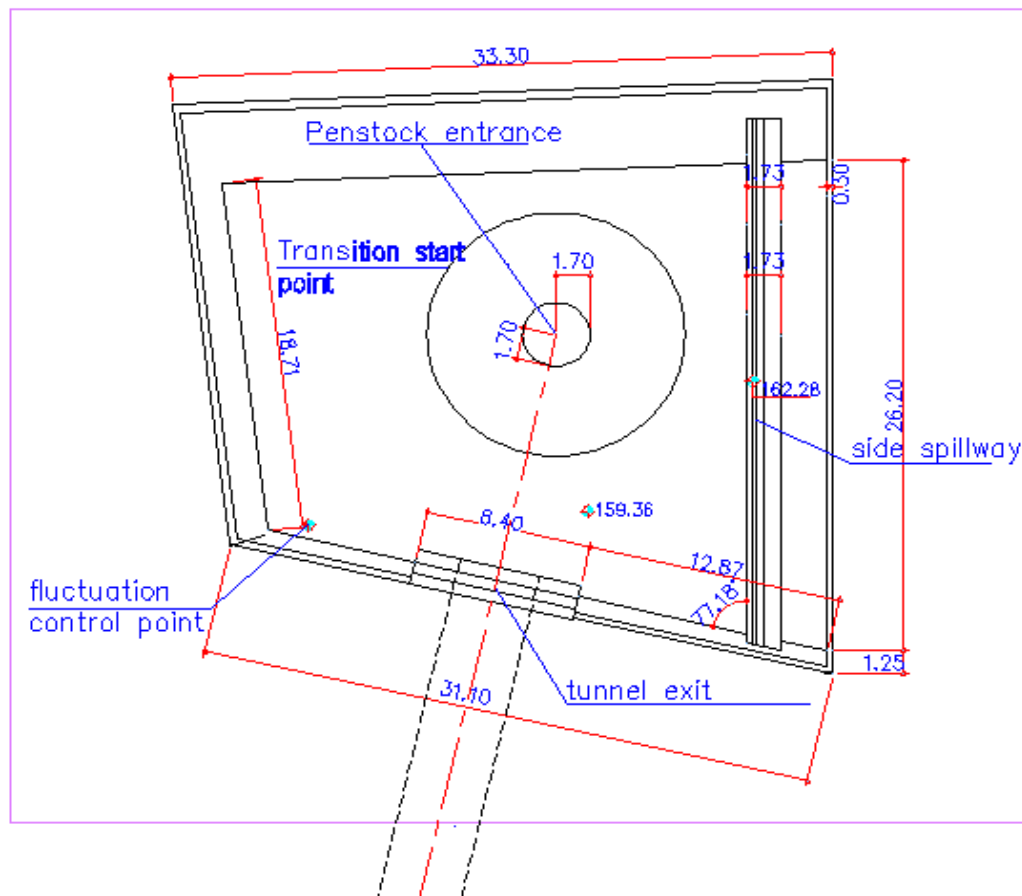
Figure 2.1 Plan view of Adacami Dam power intake. Units are in meters and degrees.
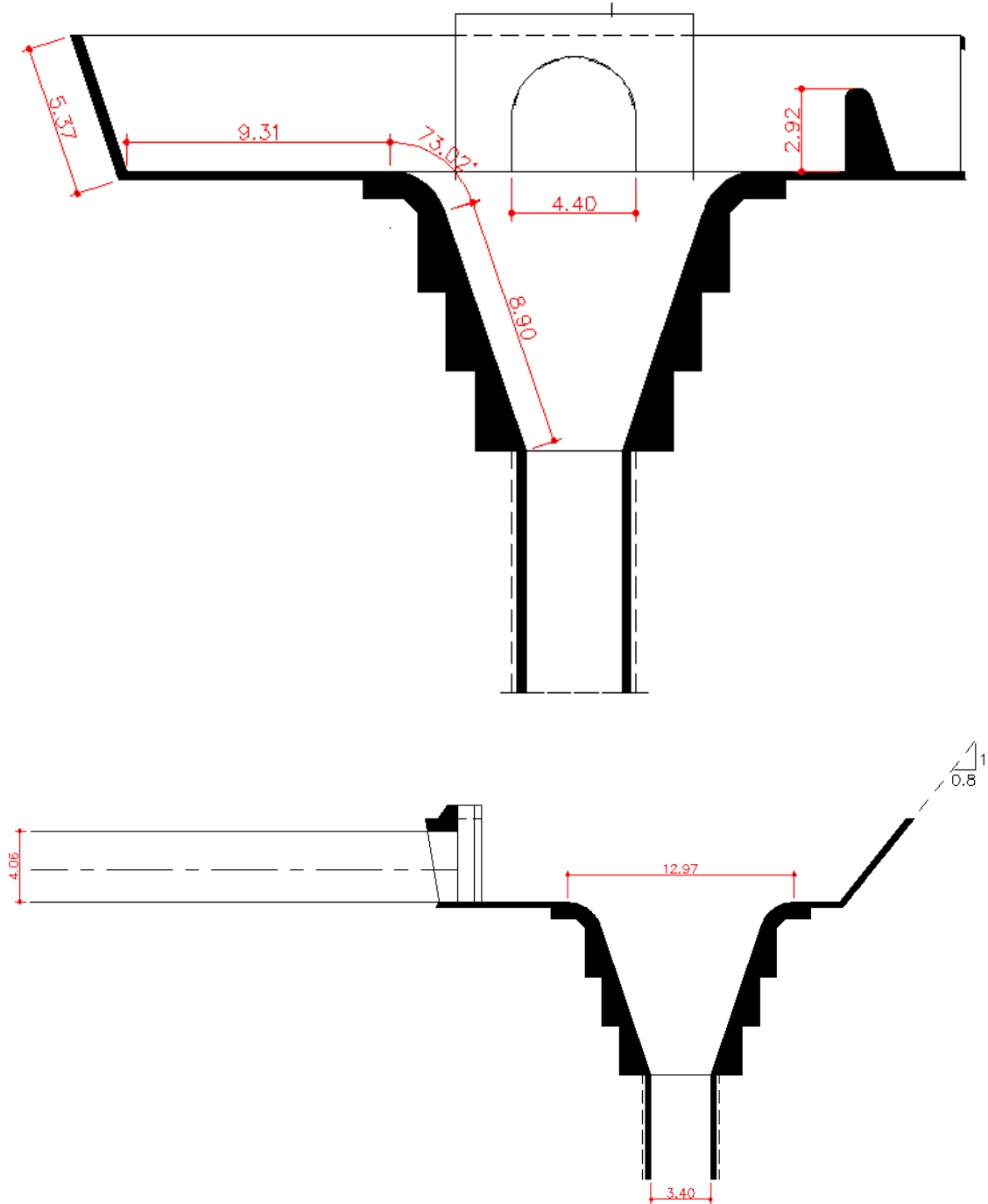
Figure 2.2 Side views of Adacami Dam power intake. Units are in meters and degrees.
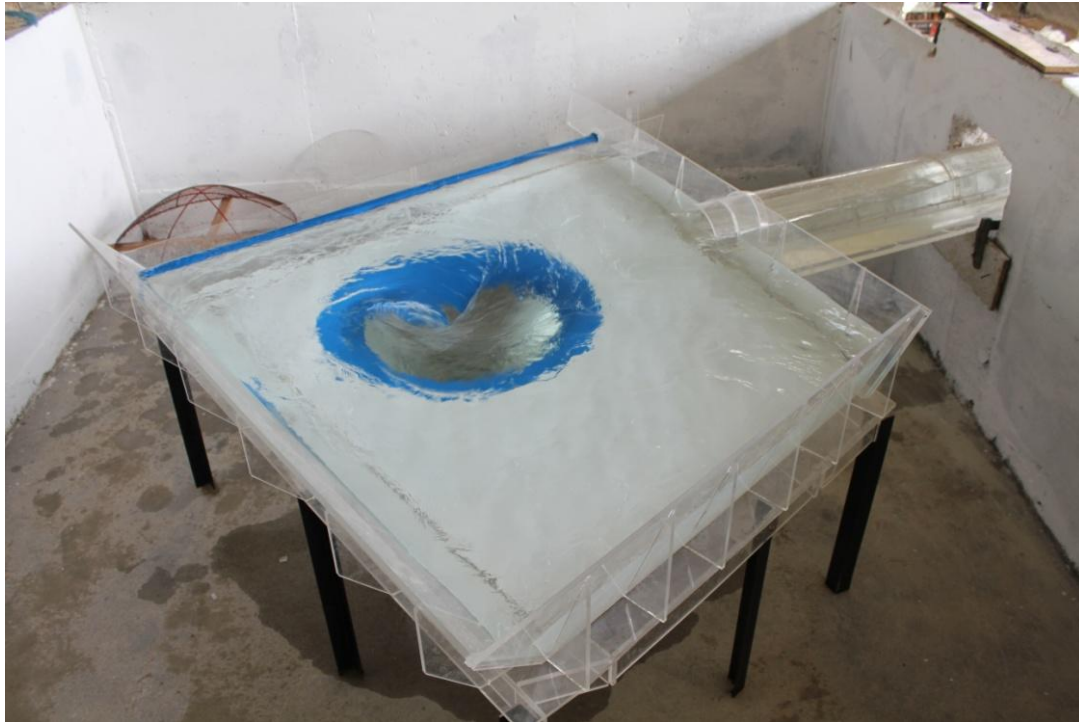
Figure 2.3 Original model setup with air core vortex formation

After repeated observations, it was concluded that the vortex formed was steady. Depression zone radially damps around entrance axis of the penstock within a margin of 0.06 meter. Air entrainment in the vortex was not continuous, however with the periods of 44 seconds, air pockets were entrained into the penstock. Fluctuations within the water surface was high, thus setting a constant water level at the side spillway was rather difficult. At a 0.912 m left to the conveyance tunnel exit, the amplitude of the surface waves were found as 0.044 m. During the experiments, minimum amount of spill was permitted and thus, for the maximum possible depth, observations were made. It was concluded that, swirl at the intake may have adverse affects on the operation of the turbine at the design flowrate. Therefore, vortex prevention methods with anti-vortex devices were considered (Aydın & Köken, 2011).

To observe the submergence effect on the intake, submergence ratio of the whole system was changed by changing the crest elevation of the side spillway. For the particular project, the submergence level can be described as the ratio of water depth in the head pond to the penstock diameter. In other words, water

depth is the critical parameter to control the vortex formation. To operate the system at the highest efficency, water level in the power intake should be sustained just at the side spillway crest level. Hence, the elevation difference between spillway crest and the bottom level of the intake gives the maximum submergence and maximum head for energy production.

Increasing submergence level is an effective way to deal with vortex formations. Greater submergence levels can be achieved by two methods, either by increasing side spillway height or decreasing the bottom elevation of the head pond. Due to practical difficulties in the model in decreasing bottom elevation, it was decided to increase the side spillway height gradually (Figure 2.4). The experiment revealed that the critical submergence level can be achieved by 0.04 meters of increase in the intake height. By increasing the elevation of the side spillway crest, fluctuations may also be controlled. Nevertheless, studies showed that the available submergence level was not adequate to diminish the fluctuations to acceptable levels.
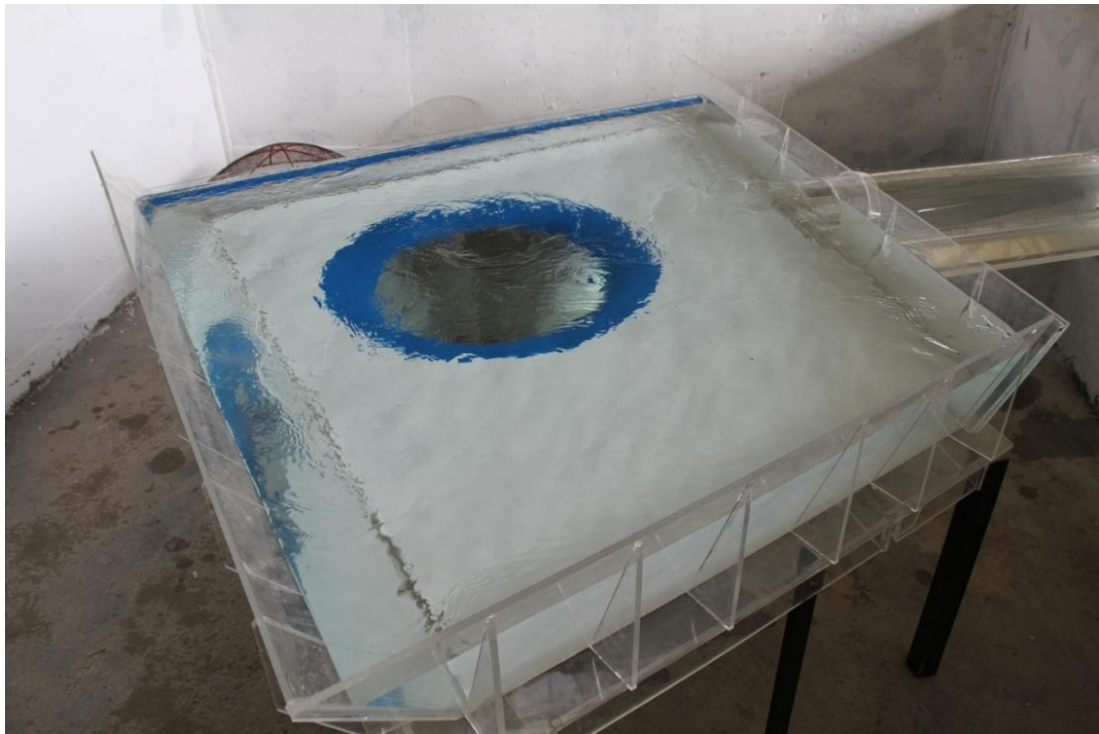
Figure 2.4 Flow conditions with increased side spillway height

2.3. Velocity and Turbulence Measurements

The study was conducted by using an Acoustic Doppler Velocimeter (ADV) device. An ADV device uses doppler shift principle, measures velocity in three dimensions. A fictitious 2-D grid of measurement points consisting of unit squares with 658 nodes was created for the model. Each unit square has the dimension of 0.050 m. In the vertical z direction, the ADV device is fixed at 0.085 m from the bottom. The device takes data from 0.050 m below its probe tips, therefore velocity field is measured at an elevation of 0.035 m from the bed (Figure 2.5).
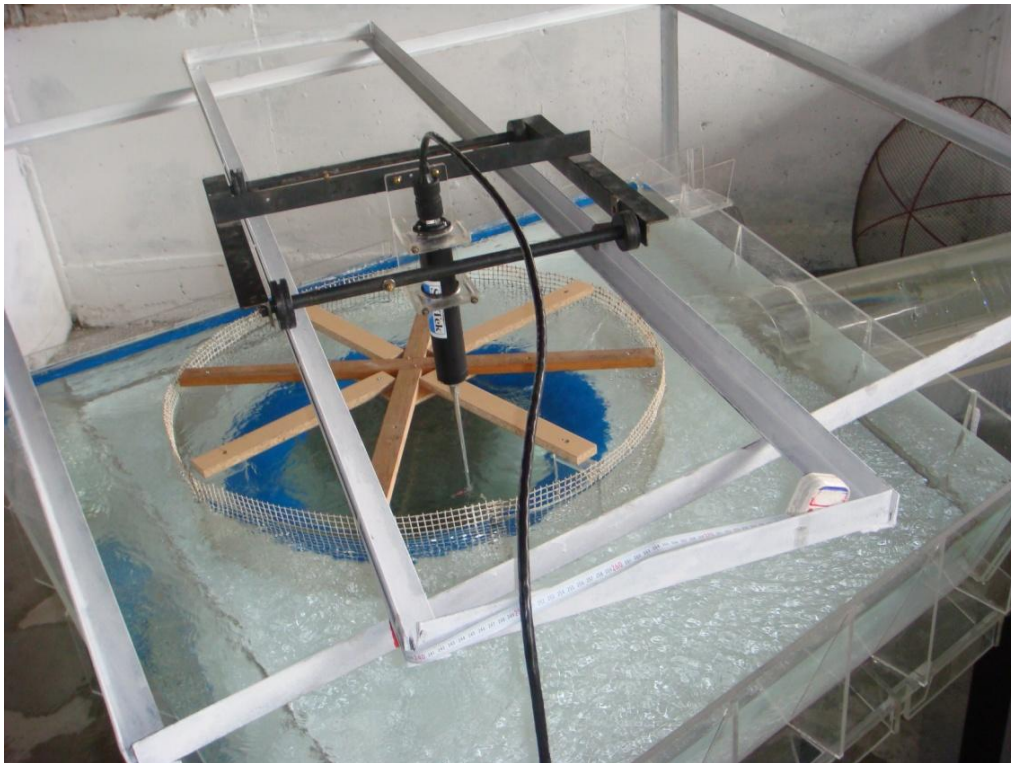
Figure 2.5 ADV device submerged into water during measurements.
The frame is shifted for movement in X direction.

In the first step, the flowrate was fixed as the design discharge of 0.023 m³/s. The submergence level was fixed into 0.160 m by adjusting the outflow valve. When the system reached the steady state; a vortex that pulls air bubbles to the intake was observed, according to the classifications (Padmanabhan & Hecker 1984). For each node, velocity values and Reynolds stresses were recorded with a digitizer sampling frequency of 25 Hz and for durations of 120 seconds. However, during the experiment, corrections were made for the received data. To remove extreme values form any data set, despiking can be applied (Goring & Nikola 2002). Recommended despiking settings were used, and the extreme values were omitted. Also, values with lower correlation score less than 70 % were deleted from the data set.

At the next step, y value was fixed to the center of the vortex core. Thus, velocity measurements were conducted along a horizontal line normal to tunnel axis. Measurements were repeated with flowrates of 0.008 m³/s, 0.011 m³/s, 0.014 m³/s and 0.017 m³/s. For each flowrate, 31 point velocity measurements were taken. Obtained data were filtered as in the first case.

Velocity vectors for all cases were plotted. For the first case, a turbulent kinetic energy (TKE) field figure was formed, based on the Reynolds stresses. The experimental results will be presented in comparison to numerical predictions in Chapter 4. TKE values were found by using the equation

$$ k = \frac{1}{2} \left(\bar{u}^1 \bar{u}^1 + \bar{v}^1 \bar{v}^1 \right) \hspace{2cm} (2.1) $$

where $\bar{u}^1$ and $\bar{v}^1$ are the turbulent fluctuations in X and Y direction respectively.

2.4. Tests with Anti-vortex Devices

To prevent both swirl formation and surface fluctuations, several anti-vortex devices were tested during the studies, namely, semi spherical screen, vertical separation walls and vertical separation walls with cylindrical screen.

2.4.1. Semi Spherical Screen

To prevent both swirl formation and circulation in the flow area and to dissipate any surface fluctuations in the system, a semi spherical screen was placed to the entrance of the penstock (Figure 2.6). Semi spherical screen bar thickness is 0.002 m and spacing between the bars is 0.016 m. The semi spherical screen was successful in preventing swirl formation, however, surface fluctuations were continued to take place in the system.

In further investigations, semi spherical screen was put into the power intake configuration with increased side spillway height. In this condition, swirl formation was prevented. Furthermore, circulations and the fluctuations in the water surface were suppressed adequately.
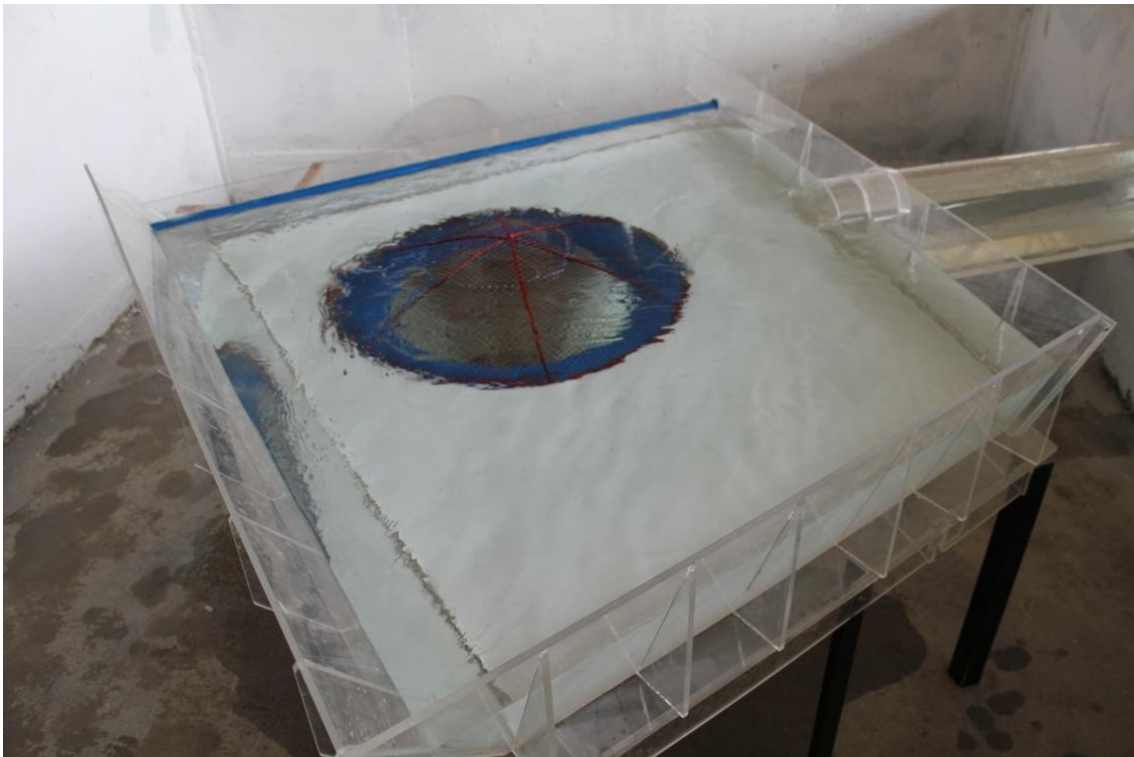
Figure 2.6 Application of semi spherical screen as an antivortex device

2.4.2. Vertical Dividing Walls

The difficulties in the production stage of a semi spherical screen was considered, thus alternative solutions were sought. To prevent the vortex formation in the penstock entrance in horizontal plane, vertical walls dividing the flow area over the intake were constructed (Figure 2.7). Separation walls formed by placing four vertical plates, forming an x like shape with respect to the tunnel axis. From the experiments, it was observed that the vertical walls prevent any swirl formation in the flow area.
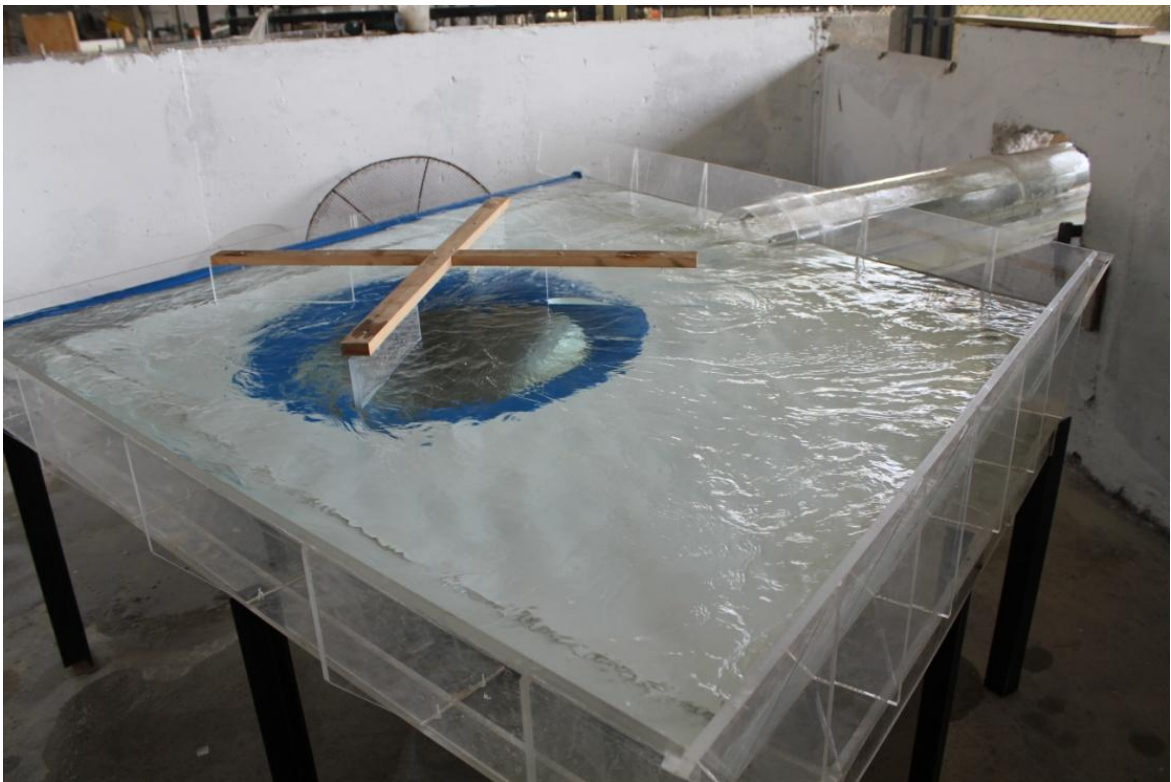
Figure 2.7 Flow conditions with vertical walls

2.4.3. Vertical Dividing Walls with Cylindrical Screen

The number of vertical walls was increased from 4 to 8 and vertical separation walls were shortened in length, when compared to the case in section 2.4.2. Furthermore, the outer ends of the vertical walls was covered by a cylindrical screen (Figure 2.8). Since the walls were shortened, they were completely positioned in the horizontal bed, without elongating to the radial transition zone. By increasing the number of walls, it was estimated that the walls would provide a rigid support to the circumscribing cylindrical screen. From hydraulic point of view, it was observed that the swirl in the power intake completely disappears with this final antivortex device. The amplitude of the surface waves were measured as 0.007 m when the water surface is at the level of side spillway crest. In the configuration, it was observed that the circulation was not suppressed adequately and the fluctuations in the surface were rather high.

As the circulation and fluctuation problem persists, side spillway crest height was also increased by 0.04 m, to increase submergence level. At this condition, amplitude of the surface waves was found as 0.002 m. Thus, the recommended structure (eight vertical walls supporting a cylindrical screen and increased side spillway crest height), have sufficient control on the water surface deformations and thus provide convenient flow conditions for safe operation of the turbines.

Figure 2.8 Flow conditions with vertical cylindrical screen

Flow conditions created by the vertical dividing walls with cylindrical screen was also considered for different submergence levels. As the submergence level decreases, naturally, fluctuations in the surface waves increase. For example, for the case with submergence depth of 0.124 m, wave amplitude was measured as 0.025 m, however, no swirl was observed within the power intake.

To observe the critical submergence level for the anti-vortex device, water level was decreased gradually. It was revealed that the minimum submergence level without vortex formation is 0.074 m. At this level, the amplitude of surface waves was measured as 0.015 m.Tests were repeated for different flow rates. As expected, the most critical case for the occurrence of fluctuations and swirl was observed at the maximum flow rate. For example, with the flow rate of 0.012 m^3/s, the flow conditions appeared to be much more smooth with less surface deformations which is more convenient for power production. The maximum wave amplitude was calculated as 0.001 m for this discharge.

CHAPTER 3

CFD CODE FLOW 3D

3.1. General Description

For perceiving and describing flow conditions in a system, aside from physical observations, numerical methods are also available. Flow fields can be simulated by using Computational Fluid Dynamics (CFD) techniques. High capacity computers are used to conduct CFD simulations. In CFD applications, the flow environment is limited by boundary conditions to simulate the surrounding effects on the particular investigation area. Nearly all CFD programs are based on solving Navier Stokes equations. As in many other commercial codes, the steps of a problem solution in using Flow 3D can be listed as follows:

a) The flow domain is defined
b) Boundary conditions are defined
c) Volume is discretized by constructing a computational grid system
d) Physical parameters are defined
e) Simulation start is given
f) A postprocessor is used to evaluate the results

Flow 3D is the CFD program used in the numerical simulation of the Adacami Dam power intakes physical model. Since version 9.4.5 of Flow 3D was used in this study, the descriptions will be based on that particular version.

The program has advanced features to simulate accurately and decrease computing time. Flow 3D has strength on simulating free surface flows. The program increases its capability by using free gridding, fractional area volume obstacle representation (FAVOR), improved volume of fluid technique (truVOF) and multi block meshing (www.flow3d.com).

Creating unstructured grids is a time consuming process. Free gridding method is creating mesh blocks with rectangular elements. This method provides fast meshing and decreased computation time. Creating meshes without considering the geometry may result in low resolution and roughness in the system. This situation was eased by using FAVOR, enabling the program to fractionally divide parts with solid region and fluid region. Furthermore, FAVOR can be used in connecting structured and unstructured grid elements. The program also improved volume of fluid technique, which had been formed and discussed by Nicholes and Hirt (1975) and Hirt and Nicholes (1981). According to the Flow 3D developers, "The VOF consist of three ingredients: a scheme to locate the surface, an algorithm to track the surface as a sharp interface moving through a computational grid, and a means of applying boundary conditions at the surface." (www.flow3d.com). The program allows to create multi block meshing, which provides flexibility for fitting meshes to geometry and creating dense meshes in particular points where precise and accurate results are desired.

Flow 3D provides ease of access to the commands and menus. In the main window, following tools were placed to provide quick access.

a) File:In file tab, it is possible to manage various operations for simulations, and workspaces, which acts as a container directory.
b) Diagnostics: Offers several options about the simulation such as creating report, solving errors and getting messages about simulation.
c) Preference: Provides choices about the customization of the program.
d) Utilities: The tab where the licensing and file compressing can be managed.
e) Simulate: The tab allows conducting simulation operations.

f) Materials: Provides material database to export material properties directly to the model.

g) Help: Provides access to the help files.

There are five titles, namely navigation, model setup, simulation, analyze and display. Navigation tab provides further options for the simulation files. Model setup is the part where the numerical model is realized. In simulate tab, simulation order can be given and various data about the simulation can be tracked such as time step, fluid surface area, mean kinetic energy etc. In analyze tab, it is possible to conduct post simulation investigations. Display tab enhances the experience by aiding visuals.

Model setup is the main part for forming the numerical model, where subsections were placed as follows

a) General: Allows adjusting finish time, compressibility, simulation units etc.

b) Physics: Where the main physical dynamics were determined.

c) Fluids: Fluids are defined and properties of fluids can be set in this part.

d) Meshing & Geometry: The part where physical geometry is formed and meshing is conducted.

e) Boundaries: Allows setting boundary conditions.

f) Initial: Helps the simulation to develop by introducing initial conditions.

g) Output: The output file can be set here.

h) Numerics: Numerical methods that are used during the simulation can be adjusted in this part.

3.2. Grid Generation and Boundary Conditions

3.2.1. Grid Generation

Before starting the grid generation, appropriate mesh size must be determined to obtain accurate results. Grid generation in the numerical model was conducted by considering several factors.

a) Grid independency
b) Computation durations
c) Render quality of defined flow regions
d) Distance from wall boundary to adjacent cells

The computational domain has to cover sufficiently large extent of flow area so that the boundary conditions applied at the upstream and downstream ends do not impose any restrictions on the free development of the flow inside the computational domain. However, oversized domains will increase number of computational mesh and therefore the computing time.

Mesh size distribution is another important aspect of CFD which directly affects accuracy of computation. The distance between the wall boundary and the first grid point next to the boundary is of primary importance in simulating the wall resistance accurately. The dimensionless distance from the wall boundary (wall Reynolds number) is defined as

$$y^+ = \frac{yu_\tau}{\nu} \qquad (3.1)$$

where y is the distance normal to the boundary, u_τ is the shear velocity. The dimensionless distance to the first grid point, y_1^+, must be kept within certain limits to obtain required resolution near the solid boundary. There are two approaches in wall region. If required, a fine grid may be used to produce full description of near wall region where y_1^+ may have values less than 4. If fine resolution in near wall region is not required then wall functions can be used to

link the first grid point to the solid boundary. In this case acceptable range for the location of the first grid point may be given as $30 < y_1^+ < 500$. Wall functions were used in the present study.

Another aspect of CFD to be discussed is the grid independency of the numerical solution. When the grid resolution is not adequate, incorrect results may be obtained. Thus, grid independency check must be conducted by obtaining numerical solutions using different grid resolutions.

Two grid systems were formed with total number of 1000000 and 432000 mesh elements. For the fine mesh, the first cell height was set as 0.005 m. Moreover, for the coarse mesh cell height was determined as 0.0118 m. With approximation of $u_\tau \approx 0.04\ U_{avg}$ initially, y_1^+ values were found by:

$$y_1^+ = \frac{y(0.04\ U_{avg})}{\nu} \tag{3.2}$$

where U_{avg} is the average velocity in the conveyance tunnel exit. U_{avg} was determined as 0.630 m/s, and ν was taken as 10^{-6} m^2/s. As a result, y_1^+ was found as 54 and 150 respectively. In grid dependency check, no significant difference was notified between fine and coarse mesh solutions. Hence, the setting shown in the Figure 3.1 was used throughout the model study.

The geometric area properties with grid generation will be discussed in Chapter 4.
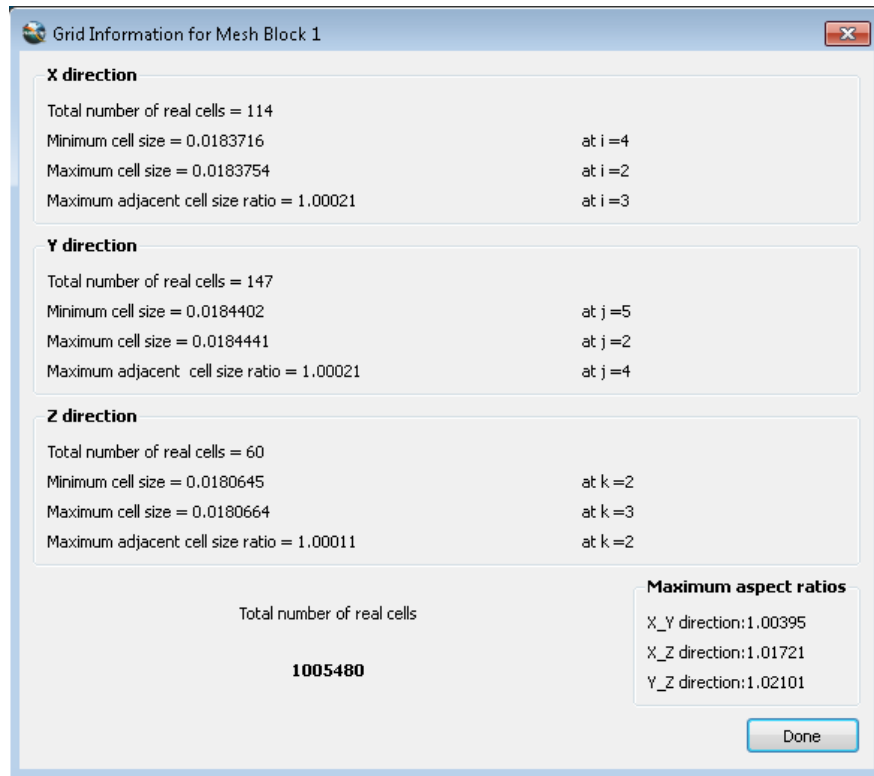
Figure 3.1 Grid information for the numerical model

Domain boundaries were set to a definite distance for allowing development of flow within the power intake area. The flow area generally consists of solid boundaries and the top part of the flow is open due to free surface flow conditions. Thus, all sides except the conveyance tunnel entrance and the penstock exit was set to "symmetry" in the grid generation program. Boundary regions can be seen in Figure 3.2, where "S" representing symmetry, "P" representing specified pressure and "W" standing for wall.
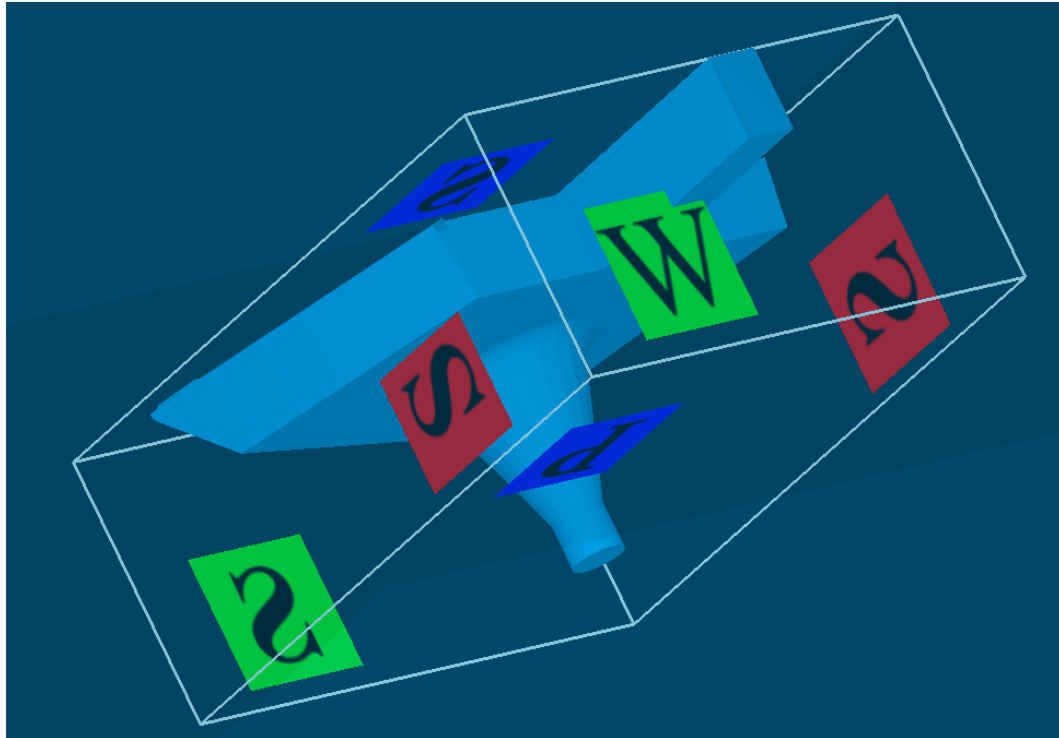
Figure 3.2 Boundary conditions of the flow region with corresponding planes

In symmetry boundary condition, no shear stresses are calculated across the boundary. Also flow and heat transfers are not allowed on the symmetry condition.

Wall boundary condition allows no flow from and to the system. However, viscous effects are calculated in wall boundary. It can also be used to set a natural boundary condition, which is the case for this study. To create natural boundary condition, wall boundary should be combined with mass source.

Specified pressure applies uniform pressure to the specified area. Specified pressure can be either constant or time dependent.

3.2.2. Boundary Conditions

In CFD, defining every component of a flow domain is practically impossible. Thus, only desired regions are solved by the computers. Boundary conditions have important role to create similar flow conditions with the physical system.

With the known values, it is not possible to determine the entrance flow depth in the conveyance tunnel. Defining an arbitrary water elevation as the inflow boundary condition by trial and error was attempted. However, to determine the final value of the water elevation required many iterations. Thus, the trial-error method was abandoned and the boundary condition was replaced with natural boundary condition. To describe natural boundary condition, developers suggest setting the boundary condition as a wall and placing a mass source just after the wall boundary condition (Flow 3D lecture notes). The boundary condition in the conveyance tunnel inlet section was built with these considerations. Mass source was directed parallel to tunnel axis by rotating the default source definition (Fig.3.2). Mass source was defined as rectangular to fit to the tunnel cross-section shape. The width of the source was set to the tunnel width. Height of the source was always chosen slightly less than the possible water depth, to reduce the number of trials.

For the outflow section of the penstock, "specified pressure" boundary condition was set to control the submergence level in the power intake. To determine the initial pressure arbitrarily, Bernoulli equation was written between bottom outlet and the free surface level. From the bottom outlet part to the surface level, depth was calculated as 0.905 m from experimental observations and this value was used to start the iterations. The losses are unknown due to the vortex formation and the velocity differences are negligible.

Thus,

$$z_s + \frac{P_s}{\gamma} = z_o + \frac{P_o}{\gamma} \tag{3.3}$$

can be used to determine arbitrary pressure level.
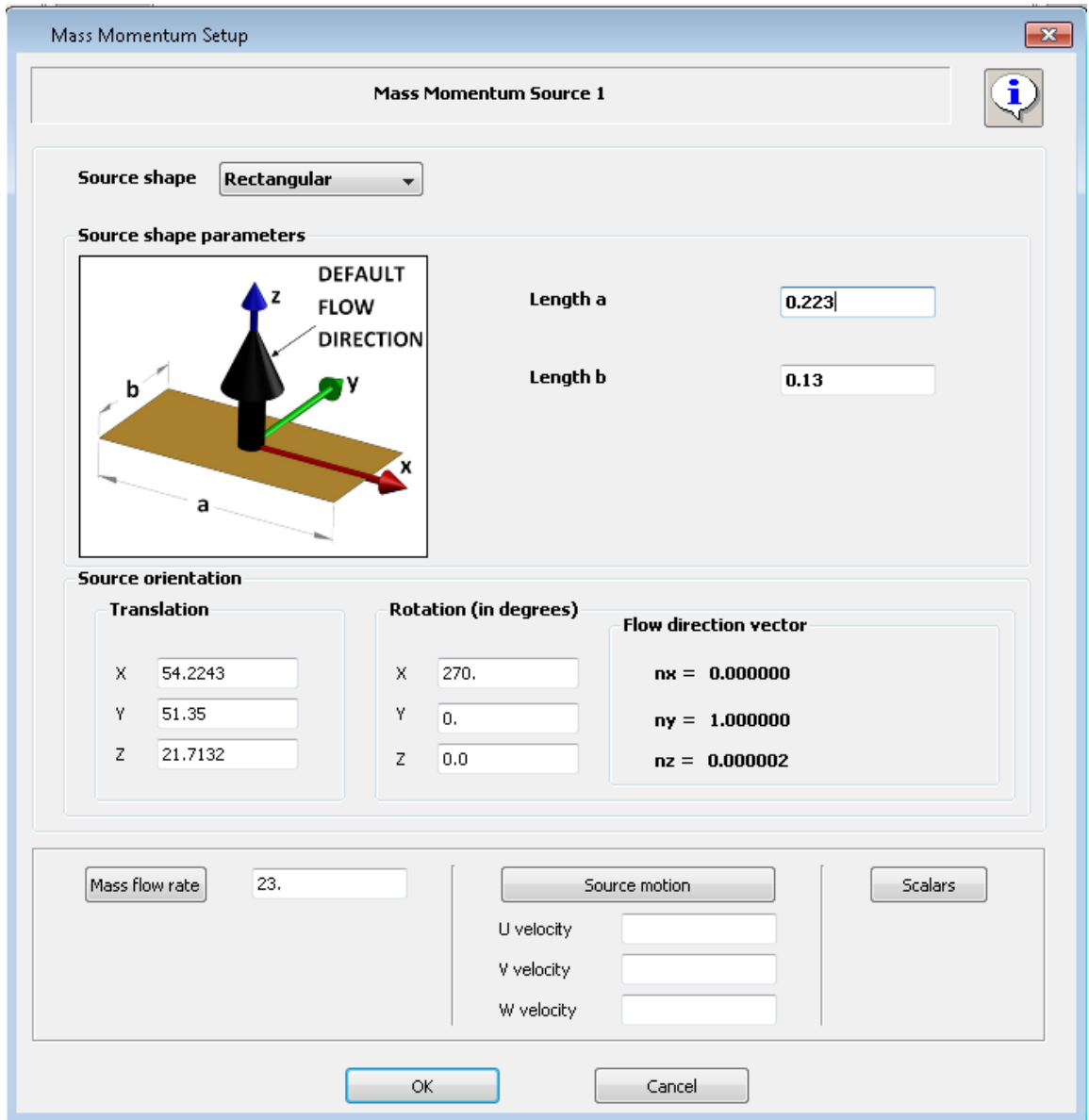
Figure 3.3 Mass momentum source setting in the system

Since pressure is zero at the free surface and z_s- z_o = 0.905 m, the boundary pressure is found as 0.905 m * 9810 N/m^3 = 8878 Pa. Pressure level iteration was started from 8800 Pa, since losses are expected. After conducting numerous simulations by decreasing pressure gradually, the experimental conditions were nearly reproduced at 7800 Pa. Hence, 7800 Pa was defined as the appropriate pressure boundary condition at the outflow section for the model.

3.3. Turbulence Model

In computation of turbulent flows, various turbulence model options are available in Flow 3D.Prandtl mixing length, one equation turbulent energy model, two equation (k-ε) model, Renormalized group model (RNG) and Large Eddy simulation model are possible options. For most of the applications, RNG models are advised for Flow 3D users (Flow 3D lecture notes). It is also mentioned that RNG model may perform better for swirling flows. Hence, it was decided that renormalized group model is the most appropriate model for the present problem.

CHAPTER 4

NUMERICAL SIMULATIONS

4.1. Numerical Simulation for the Original Design

To form the numerical model, the first step is to construct a 3D model of the system in computer environment. In Flow 3D, geometric description of the flow domain can be conducted. However, since the power intake design has a complex geometry, the 3D model was prepared in AutoCAD. In AutoCAD, drawing file should be formed in 3D layers with 3D solid form. Subsequently, the drawing can be imported into Flow 3D as a file with 'stl' extension. In the numerical model, the side spillway was removed and replaced with a vertical wall, due to the difficulty in describing spill boundary condition for a continuously up and down moving free surface. Therefore, the small amount of spilled water allowed in the physical model was set to zero in the numerical model. Thus, it was thought that the submergence level in the intake can be controlled by outflow pressure boundary condition that was discussed in section 3.2.2.Before starting to draw, boundaries of geometry had to be defined. Since the power intake pool must be covered as a whole, inlet and outlet parts of the intake should be truncated by imposing appropriate boundary conditions. Adequate conveyance tunnel length to be included in the numerical solution was chosen as 1.2 m in the model scale to allow free development of the flow at the inlet section. The outflow boundary was placed just after the geometric transition to the circular penstock, to keep the size of the computational domain reasonably

small and save computational time. The horizontal coordinates were chosen such that Y-axis was parallel to tunnel axis and X-axis was normal to it with the origin located at the tunnel exit.

In the first attempts, solid regions were modeled with actual wall thicknesses in the physical model. When the drawings were imported to the program, it was observed that wall thicknesses were not adequate to be rendered by the grid program. Hence, wall thicknesses were increased and file was imported again. In the second attempt, it was observed that there were so many void mesh cells, which may elongate simulation duration unnecessarily. In addition, difficulties were encountered while defining boundary conditions. After several trials, it was decided to create a complementary volume. In Flow 3D, by defining a flow region as a "complement", one can interchange solid and void regions. In other words, complement behaves as a "negative" of the original implemented file. Hence, flow volume was formed with solids in AutoCAD, and imported as a complement file to the Flow 3D program.

A single block mesh was formed by covering the complete flow domain (Figure 4.1). Various aspects of grid generation and mesh properties were discussed in the previous chapter, in section 3.2.
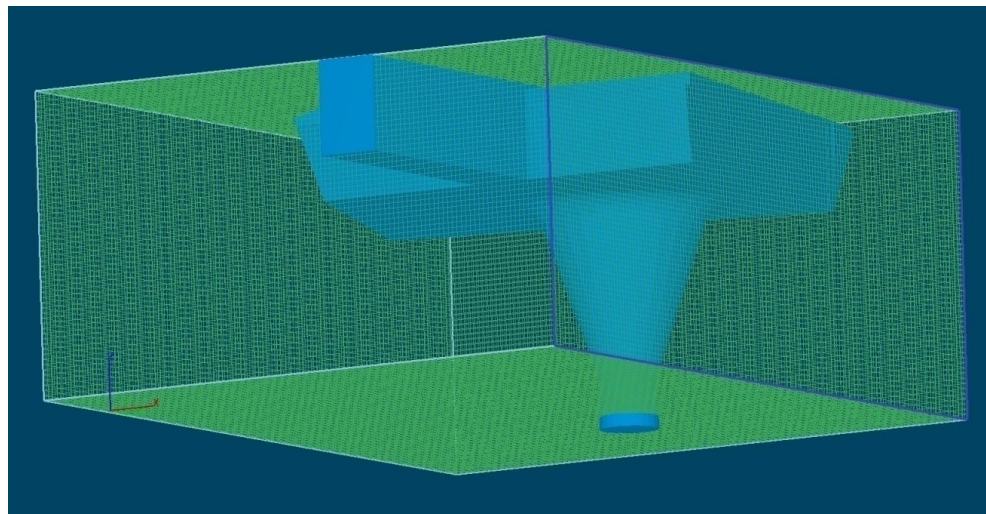
Figure 4.1Flow region with complement drawing and meshing. All mesh boxes outside the flow volume are solids.

In the physics tab, gravity was defined in negative z direction by entering -9.81 m/s^2. Mass source, boundary conditions and viscosity definitions were discussed in sections 3.2.2 and 3.3 respectively.

As the fluid, "water at 20°C" was chosen and loaded from materials tab. Initially, intake was submerged in water to the side spillway crest level of the physical model. In numerical tab, momentum advection was changed to third order, since the developers suggest that swirl problems can be analyzed most accurately by using third order momentum advection (Flow 3D lecture notes).

In Flow 3D, steady state is assumed to be reached when variations of average mean kinetic energy and average mean turbulent energy with respect to time became less than 1 %. All simulations were continued to reach the steady state condition. However, for the original design case the steady state (determined by the code itself) was not reached. For this particular case, although the simulation run time was extended up to 300 seconds (much longer than a typical runtime), it was not possible to get the steady state message from the solver. When the flow parameters were monitored as function of simulation time it was noticed that water surface and discharge were periodically oscillating (Figure 4.2). Oscillation of the free surface was very similar to the case observed in the physical model. From Figure 4.2, it was observed that the system has a tendency to decrease the submergence level first by a rapidly increasing outflow in the system. Balance between inflow and outflow was reached after nearly 70 seconds of simulation time. However, flow was oscillating at about 3 s of oscillation period with nearly 0.001 m^3/s amplitudes in discharge. Similar oscillations in free surface were also observed. Hence, at least 70 seconds of simulation time was needed to reach the oscillatory steady state.
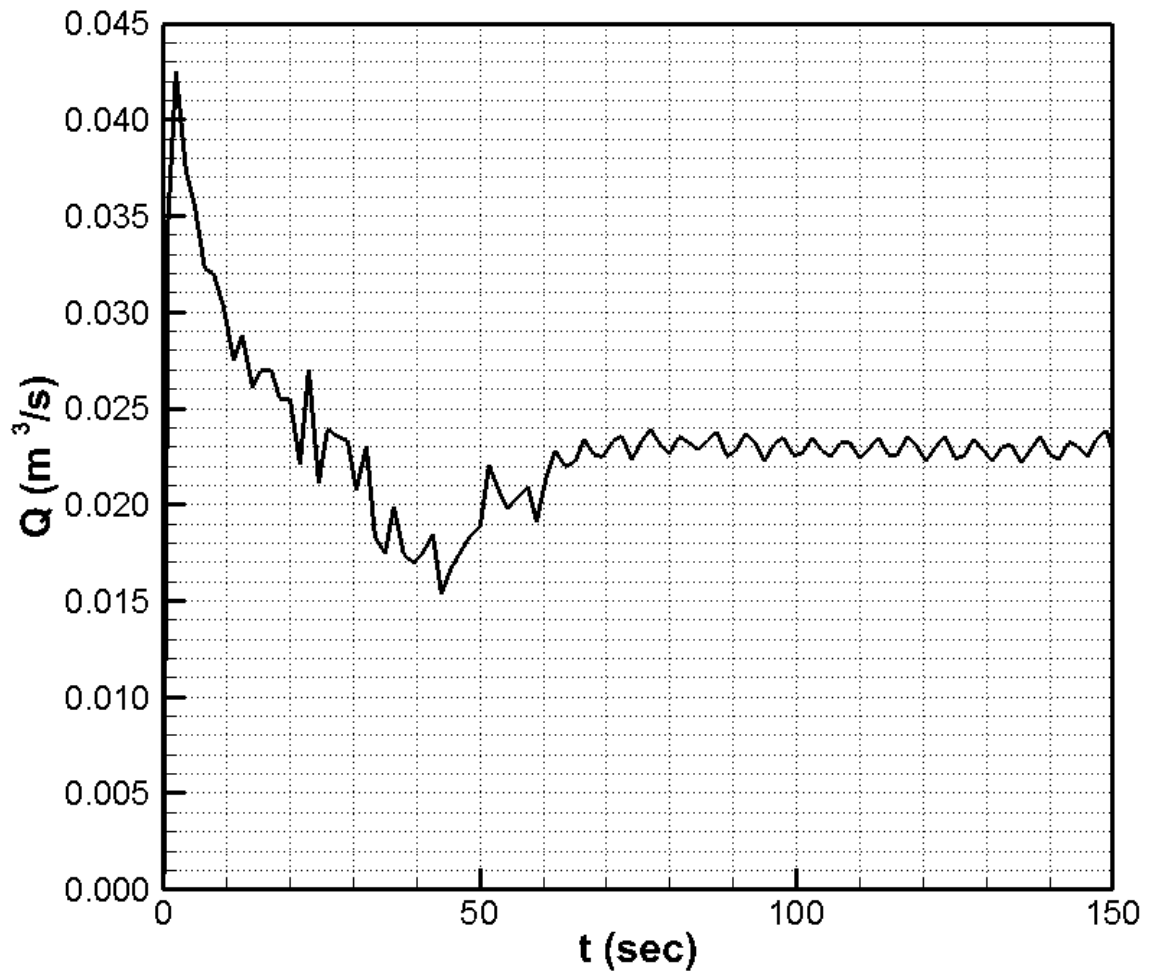
Figure 4.2 Discharge variation during numerical simulation

For the design discharge (0.023 m^3/s), the comparison between the measured and computed velocity fields is shown in Figure 4.3. It can be observed that Flow 3D is successful in simulating vortex flow within the power intake. In general, the velocity vectors in the main stream are consistent with the measured ones. Major differences in the direction and magnitude of velocity vectors are observed around the vortex core. This difference can be explained by several contributing factors to the error. The error due to the measurements by the ADV device, removal of the side spillway in the numerical model, errors due to the meshing, roughness due to the rendering issues, and high free surface fluctuations in the particular area can be listed as the contributing factors.

The computed and measured turbulent kinetic energy (TKE) values were also compared. Data were collected from 3.55 cm above from the bottom layer. Contour plots of TKE are shown in Figure 4.4. Calculated values are consistent with the measurements. As in the velocity field comparisons, in the core region differences can be noticed. During near core region measurements, high fluctuations occasionally disturbed the measurements which may be the cause of turbulent kinetic energy difference.

Comparisons of velocity field over the X-axis were repeated for smaller discharges other than the design discharge. Computed and measured velocity vectors along a line parallel to X-axis passing through the vortex origin are shown in Figure 4.5 for various flow rates. Good agreement is observed outside of the vortex core. Swirl in the intake got stronger with increased flow rates. In low flow rates, magnitudes of vectors of numerical case are greater than measured cases; whereas opposite is valid for high flow rates. ADV measurement errors become more significant at low velocities. In addition, creating the same state of flow for smaller discharges had been difficult in the experimental setup due to unsteadiness. Furthermore, the core depression level of the vortex is not constant, i.e. unstable vortex formation was observed which may cause inaccuracy in the measurements.
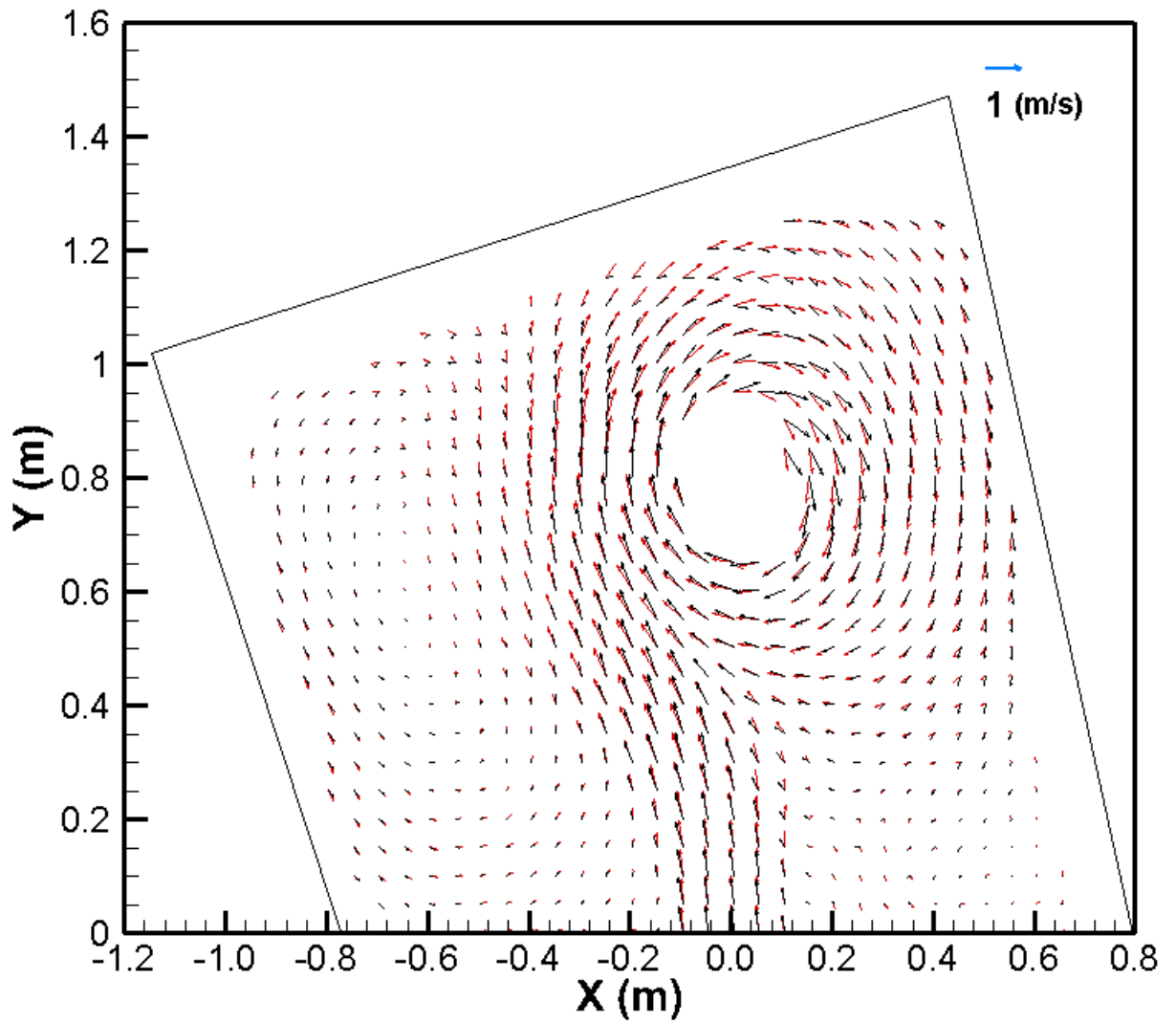
Figure 4.3 Comparison of velocity vector field (→ Measured→ Computed)
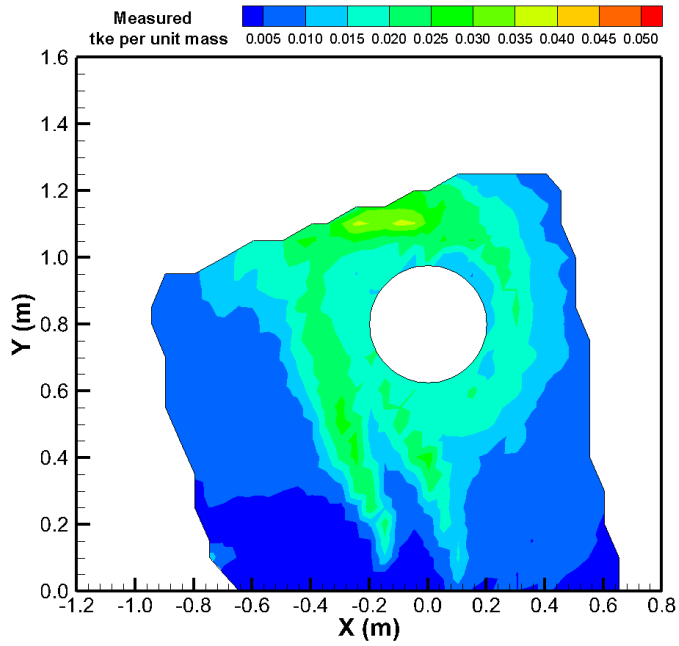
a) Variation of measured turbulent kinetic energy in the flow domain
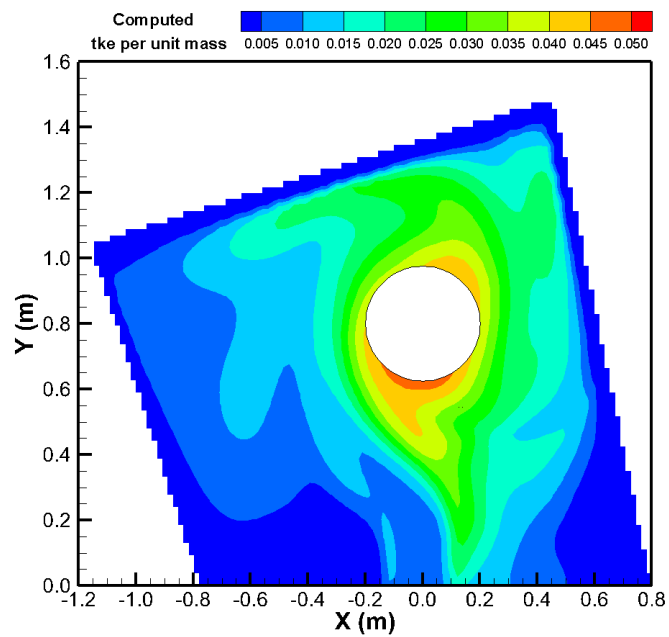
b) Variation of computed turbulent kinetic enery in the flow domain

Figure 4.4 Comparison of turbulent kinetic energy (m^2/s^2).
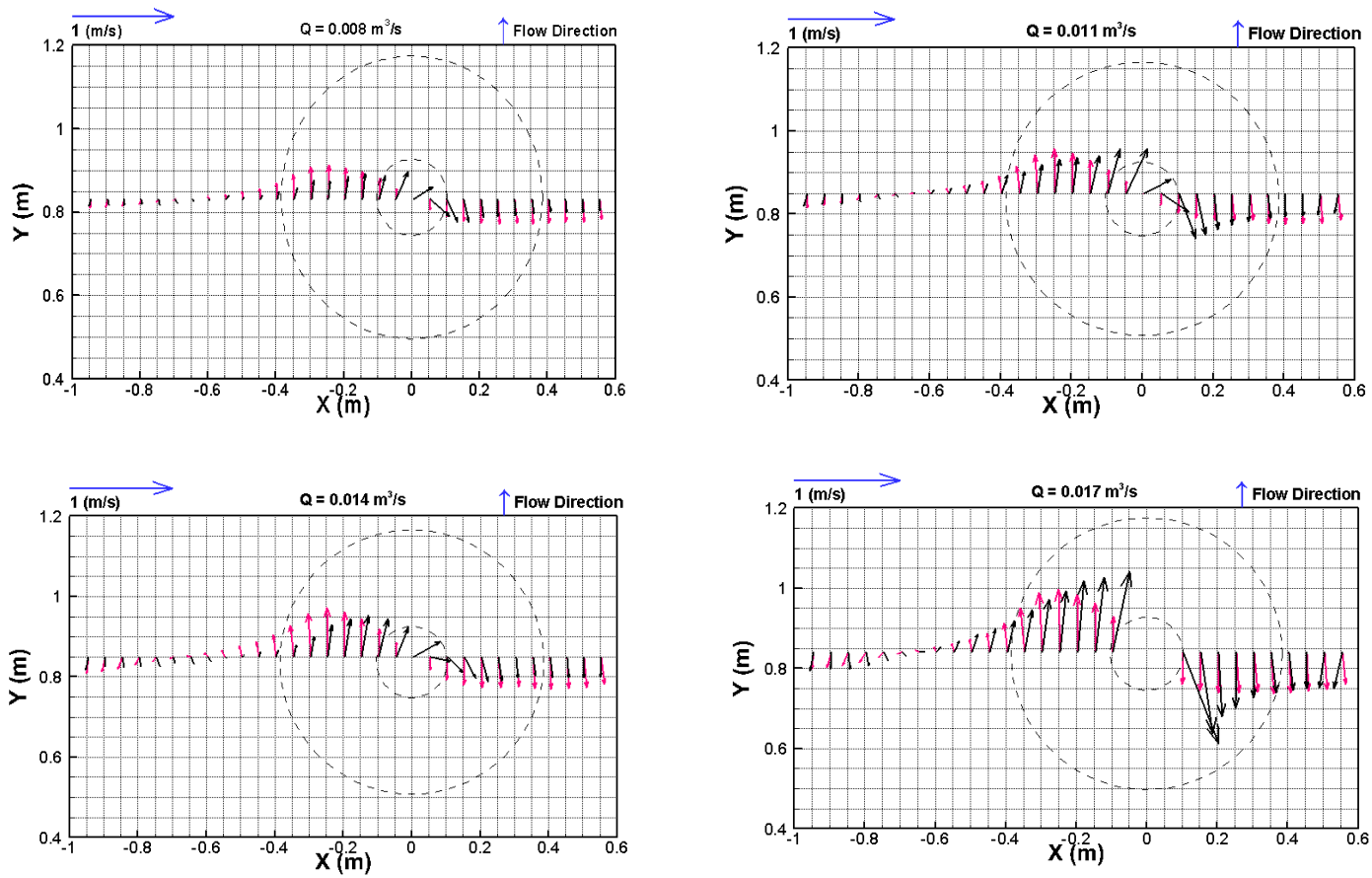
Figure 4.5 Velocity distribution along x axis, passing through the center point of the vortex. (→ Represents vectors from experimental data → Represents vectors from numerical data)

Comparisons of the computed and measured turbulent kinetic energy values along the same axis are shown in Figure 4.6. The general agreement is again quite satisfactory. However, there are some peak values observed in the measured data which do not exist in the computations. The measured peak values may be in error due to insufficient seeding in water and filtered data.
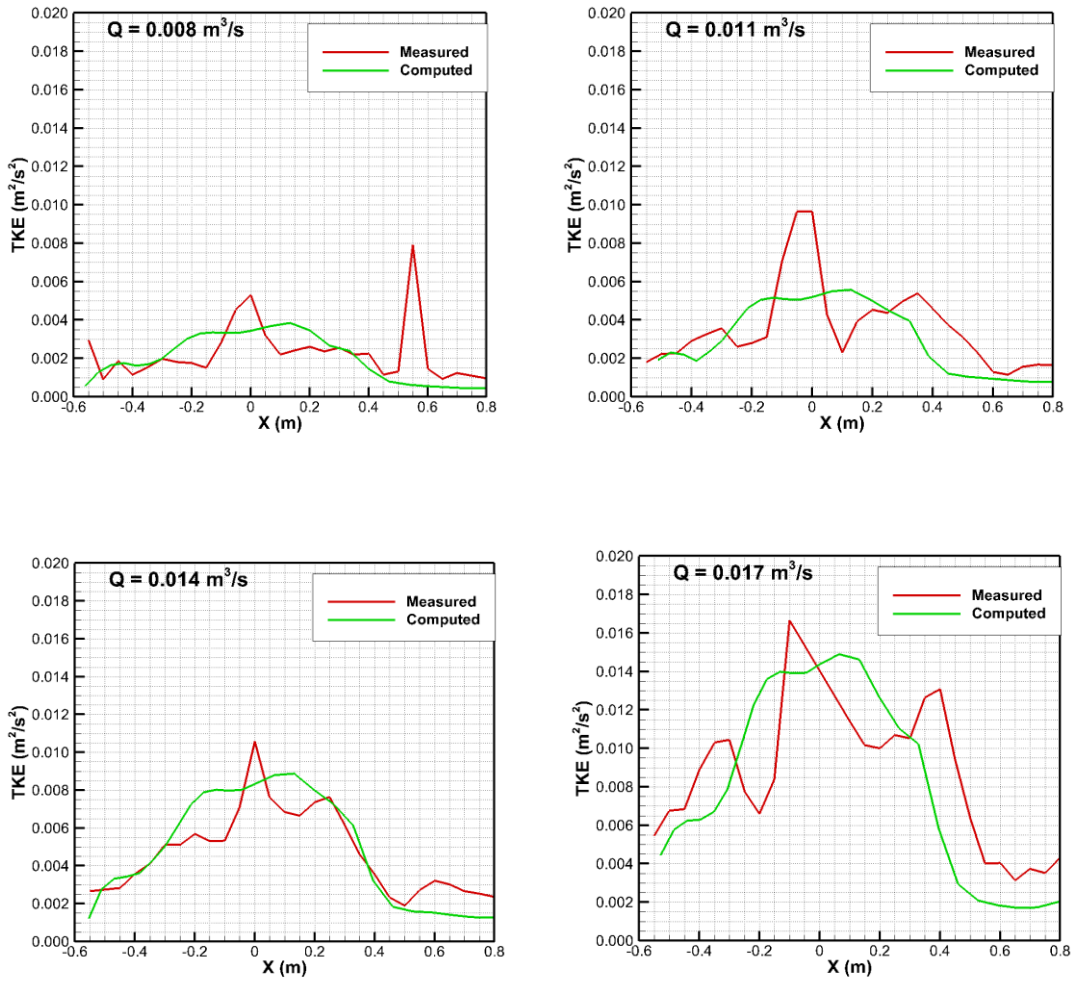
Figure 4.6 Comparison of turbulent kinetic energy values for different discharges.

4.2. Evaluation of Vortex Strength

In all intake structures, there may be a certain degree of risk for occurrence of vortices. In general, Froude number is used to express the risk of vortex formation. Usually, the required submergence depth to avoid vortex formation is expressed in terms of the Froude number. For the present problem the submergence Froude number is defined as.

$$F_r = \frac{V}{\sqrt{gs}}$$
(4.1)

where V is the average velocity in the penstock, s is the submergence depth. In the present study, the measured and computed velocity fields and free surface deformations are available. Therefore, a more precise measure of vortex formation can be given. Potential function for an ideal (inviscid) vortex is defined as(Potter et al., 1997)

$$\phi = -\frac{K}{2\pi}\theta$$
(4.2)

where ϕ is the potential function, K is the vortex strength and θ is the angular variable. The velocity component in θ direction can be obtained as

$$u_\theta = \frac{K}{2\pi r}$$
(4.3)

where r is the radial position. The unit discharge on a horizontal plane between two radial positions, r_1 and r_2, can be obtained from integration of the velocity component.

$$q = \frac{K}{2\pi}\ln(r_2/r_1)$$
(4.4)

This last equation can be re-written to evaluate vortex strength, K, from the measured or computed velocity field by defining appropriate r_1 and r_2 values.

$$K = \frac{2\pi q}{\ln(r_2/r_1)}$$
(4.5)
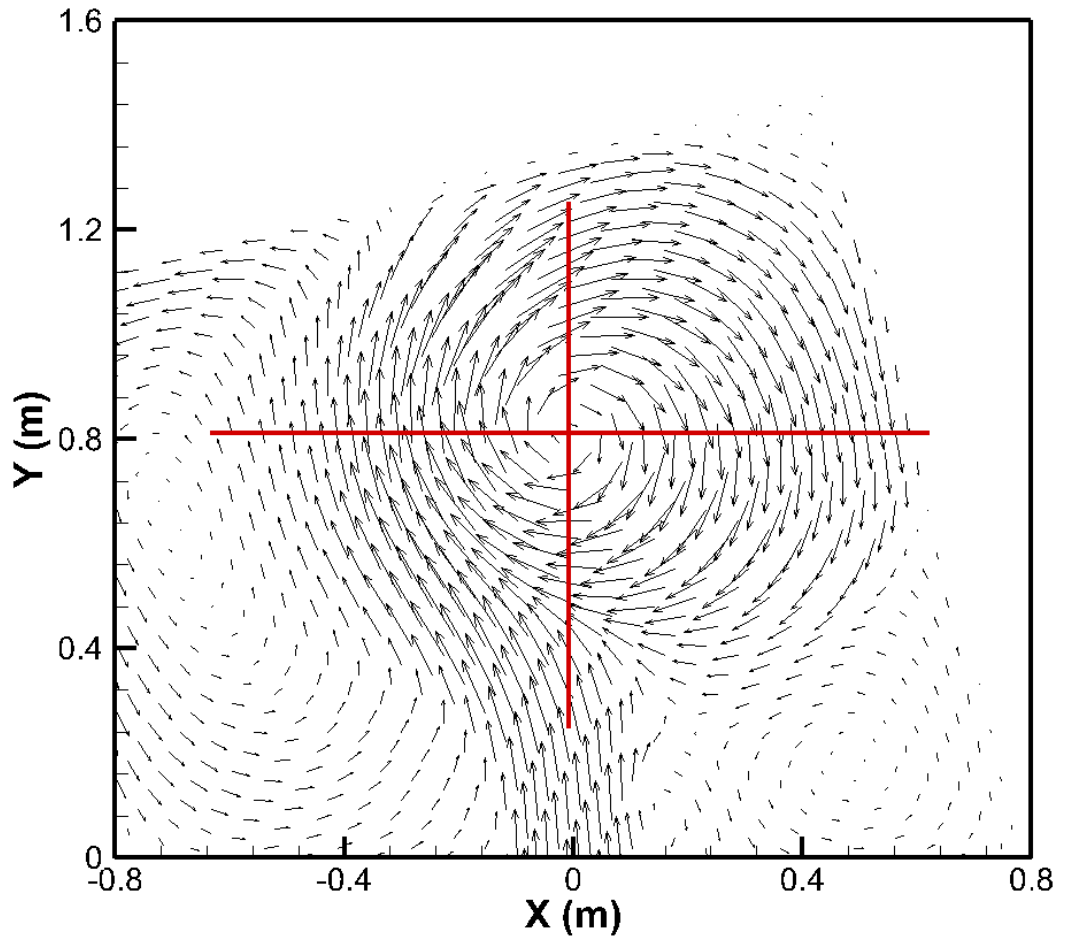
Figure 4.7 Determination of vortex strength K by integration in radial
directions parallel to four orthogonal axis lines.

r_1 values were determined by considering vectors just after near core boundary. r_2 values were limited by interfering flow conditions. Vortex strength K was calculated along lines that parallel to the grid axes (+X, +Y, -X, -Y). The reason to choose axes for calculation of K is to use Cartesian velocity components in integration (Figure 4.7). Velocity components at 30 points were extracted for each line, and integrated to obtain the unit discharge. Velocities near the vortex core not considered due to possible errors in that area.

K values obtained from each coordinate direction were then averaged to obtain a mean value to eliminate variations due to asymmetry of the vortex.

To evaluate the vortex strength from the computational velocity field Flow 3D output files were imported to a graphics program. Slices taken were adjusted to show velocities in the vector form. The vector fields were interpolated for the velocity measuring points in the physical model. Afterwards, triangulation was conducted to extract data from spaces between vectors, with method of linear interpolation.

Odgaard (1986) stated that K value should be independent from z coordinate. To check the independency of K value, computations were repeated at different depths. The sliced planes were located at 0.03 m, 0.06 m, 0.09 m and 0.12 m from the bottom.

In Figure 4.8, it can be observed that computed K values are nearly constant up to 9 cm of water depth. As the integration plane approach to free surface, the contribution of the vortex core to the integral is limited therefore, K value decreases in case of 12 cm depth. In the following sections, K values are computed at 3.55 cm from the bottom which is the depth of ADV measurements.
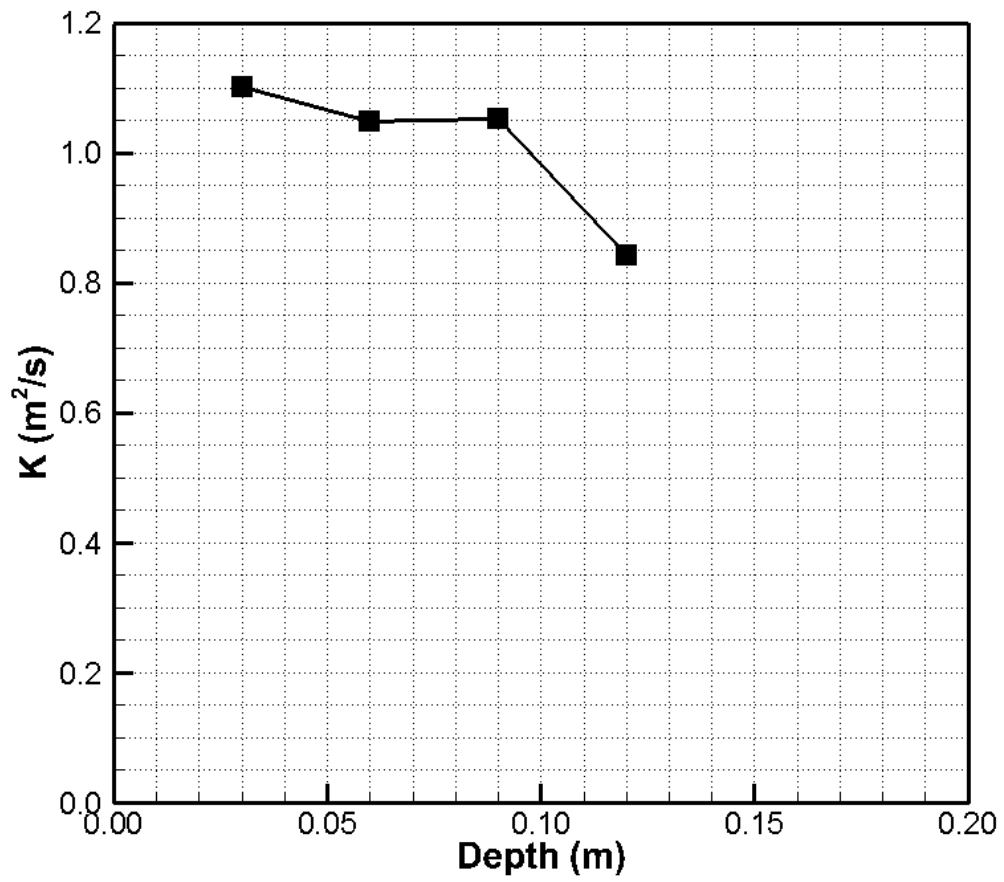
Figure 4.8 Vortex strength as a function of the depth of computing plane.

The vortex strengths evaluated from computed and measured velocity field for the original intake design are shown in Figure 4.9. In the experiments, water level in the intake pool was kept constant being equal to the side spillway crest elevation. Therefore, in the numerical solutions the outflow pressure boundary condition is adjusted to obtain water levels always equal to the same value for varying discharges. It is observed that the vortex strengths obtained from the numerical solution and measured velocity field have similar dependence on the Froude number. There are large differences between vortex strengths at low flow rates but the difference between the two decreases to 15% with increasing discharge.
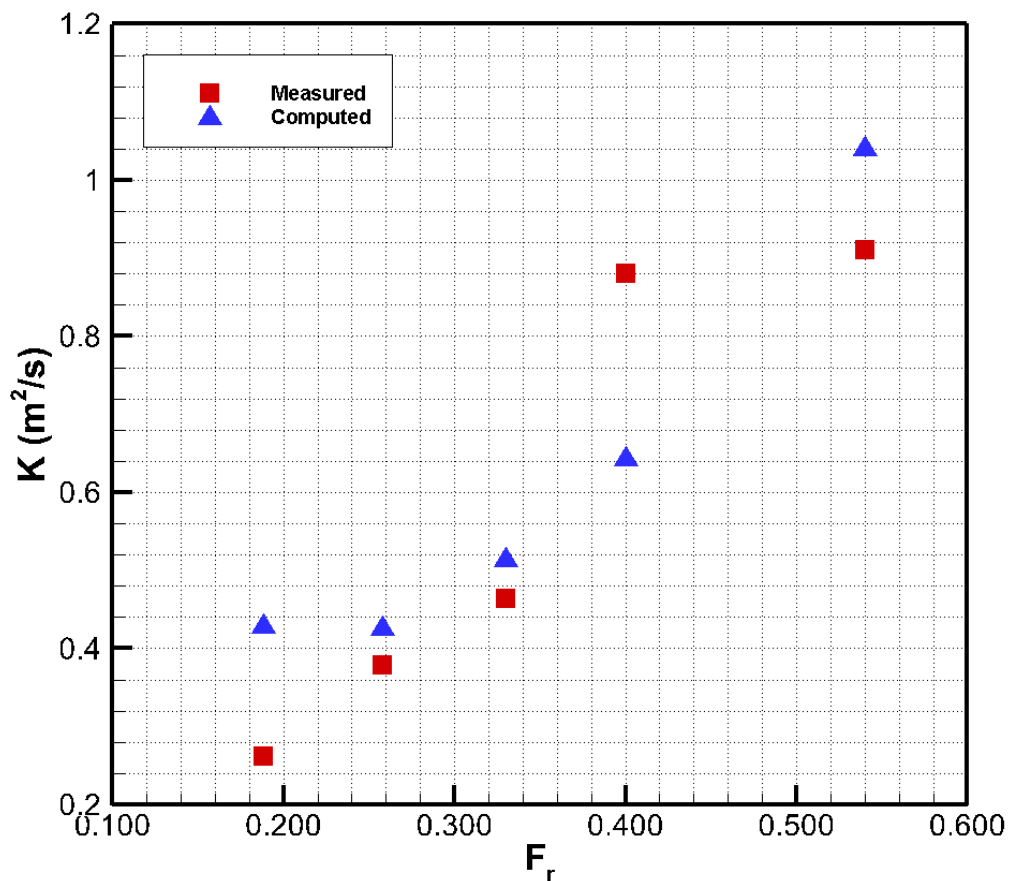
Figure 4.9 Vortex strength K for the original design evaluated from the computed and measured velocity fields

The vortex strengths computed for the design discharge with variable submergence depths are shown in Figure 4.10. Computations were performed by changing the pressure boundary condition at the outflow boundary. Vortex strength increases with Froude number with increasing slope at high Froude numbers. Vortex strength obtained from measured velocity for the side spillway submergence level is also indicated as a single point on the figure. It is not so easy to determine the critical value of the vortex strength just by observing its dependence on the Froude number. Free surface profiles along the tunnel axis passing through the vortex core (Figure 4.11) are very helpful to visualize the flow conditions corresponding to data points of Figure 4.10.
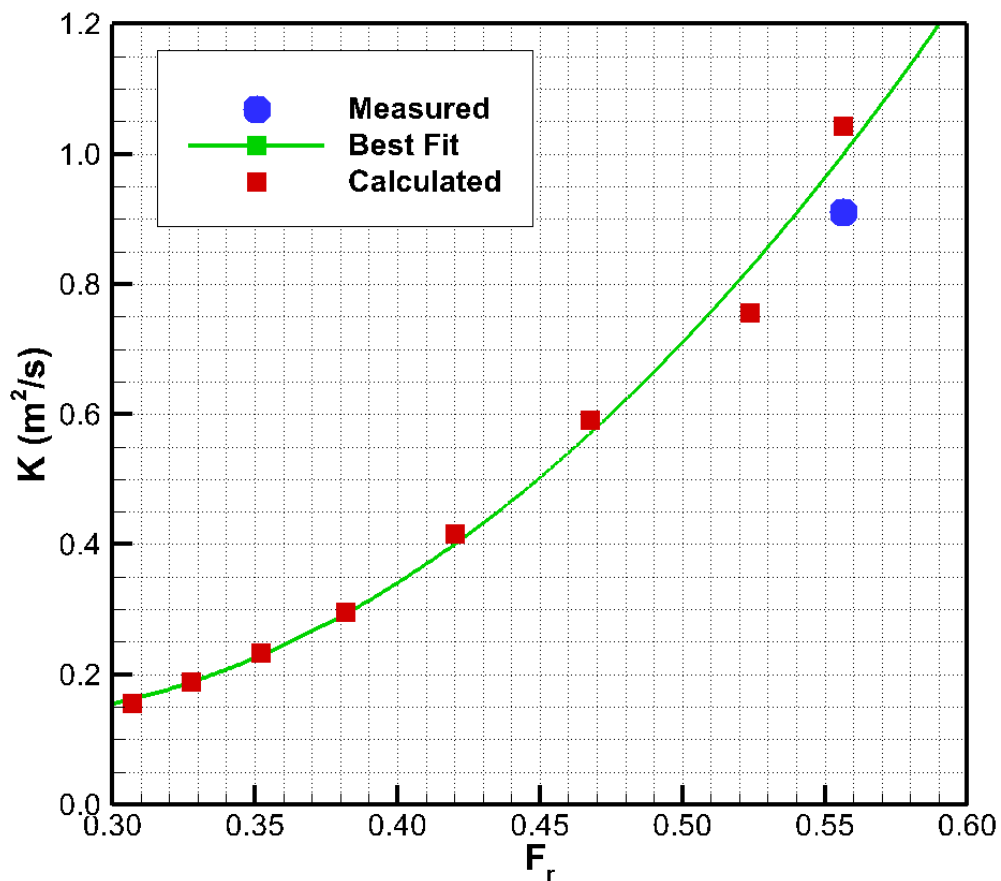
Figure 4.10.Vortex strength K for the original design computed for the design discharge for variable submergence depths

The maximum submergence is obtained for the maximum outflow pressure (12000 Pa) for which free surface is nearly flat and vortex strength is minimum with a value of 0.152 m^2/s. A noticeable surface depression is observed for the outlet pressure of 10200 Pa which produces a vortex strength of 0.3 m^2/s at F_r= 0.38. Therefore, the critical vortex strength for the present intake geometry at the design discharge can be set as K=0.3 m^2/s. The submergence depth for the critical vortex strength is approximately 33 cm. Numerical data for the simulations for the design discharge are shown in Table 4.1.

Table 4.1 Numerical data for the design discharge

P_{out} (Pa)	K (m^2/s)	s (m)	F_r
7800	1.042	0.154	0.557
8400	0.755	0.174	0.524
9000	0.591	0.218	0.468
9600	0.415	0.270	0.421
10200	0.295	0.327	0.382
10800	0.233	0.385	0.352
11400	0.188	0.445	0.328
12000	0.155	0.506	0.307
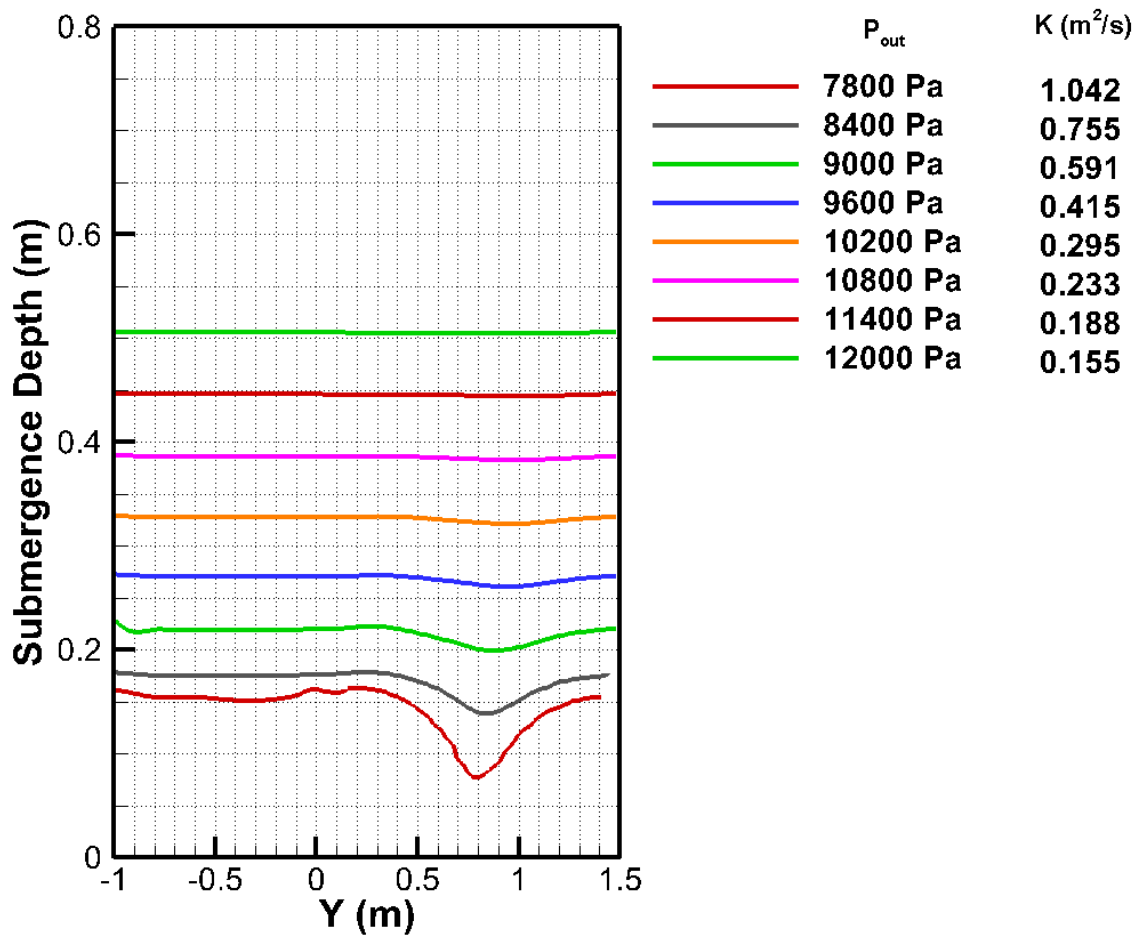
Figure 4.11 Free surface profiles along the tunnel axis computed for the design discharge for variable submergence depths

4.3. Simulations with Idealized Domains

To investigate the vortex generation in different intake geometries, simulations were conducted on idealized domains. The boundary condition settings and the solution methods are all the same with the original design configuration, except the side wall geometry of the head pond.

4.3.1. Square Shape

First, an idealized domain was created by replacing the quadrilateral shape with a square shaped intake. The positions of the conveyance tunnel and the penstock connection were the same. The side length of the square was determined by considering the horizontal distance between the penstock entrance and the conveyance tunnel exit, measured as 0.408 m. The distance was determined as the half-length of the square pool side length. However, it was observed that the square formed was not adequately wide. Hence, side lengths were doubled. The square shape with a_s = 1.632 m side length was placed with its center corresponding to the center of the penstock entrance. Simulations were conducted with the same settings of the original design and the same mesh size with the design discharge value of 0.023 m^3/s. Bottom outlet pressure was set to 7800 Pa. However, it was revealed that symmetrical flow occurs within the square domain with no vortex (Figure 4.12). To investigate flow behavior in an eccentric orientation, the square pool was shifted by 0.05 a_s to create eccentricity on the system. No vortex formation was observed and symmetrical flow conditions persisted within the system. To further distort the flow, square region was rotated by 15°in counter clockwise direction around the Z-axis. However, flow conditions did not change. Finally, an artificial external excitation was applied by introducing an initial vortex by shifting the mass source into the pool area and eccentrically placing to the corner of the pool. After simulating 30 seconds of flow with the eccentrically placed mass source, the mass source carried to the original position and simulation continued. The aim to

conduct this simulation was to observe whether the code would be able to sustain the externally formed vortex. Studies revealed that as the flow developed, the vortex was disappeared again. It was decided that further studies are needed and physical model may be constructed to investigate actual flow behavior.
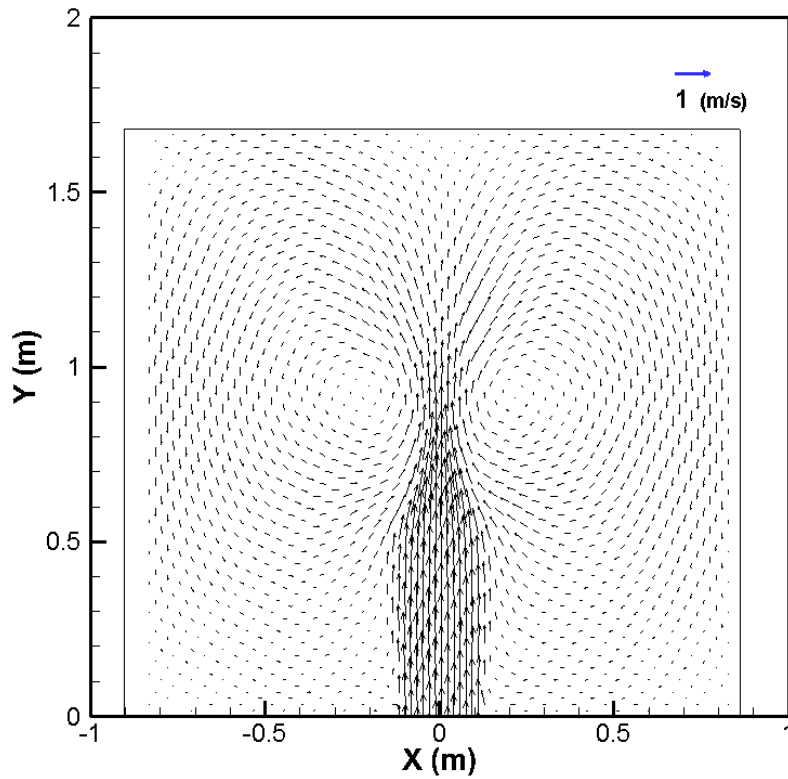
Figure 4.12 Velocity vectors for the square flow domain with inlet discharge of 0.023 m^3/s

4.3.2. Cylindrical Shape

Another investigation was conducted by replacing the square domain with a cylindrical. Diameter of the cylinder, r_c, was determined as equal to a_s, which was 1.632 m. Cylinder was placed in a position that the central axis of the cylinder coincides with the penstock entrance center. The conveyance tunnel and the outlet section kept in the same coordinates. The same mesh size and settings were used and simulations were repeated with the design discharge value of 0.023 m^3/s. The bottom outlet pressure was set to 7800 Pa. It was observed that two vortices were formed. Vortex strength was calculated for stronger vortex case. K values were calculated as described in the previous sections. However, three axes were considered during the calculation of K. +X direction was omitted due to the jet interference caused by conveyance tunnel. Slices were taken from 0.035 m, with bottom surface level of the pool is considered as datum. Free surface elevation was determined over the axis located in the center of the conveyance tunnel (Figure 4.12).
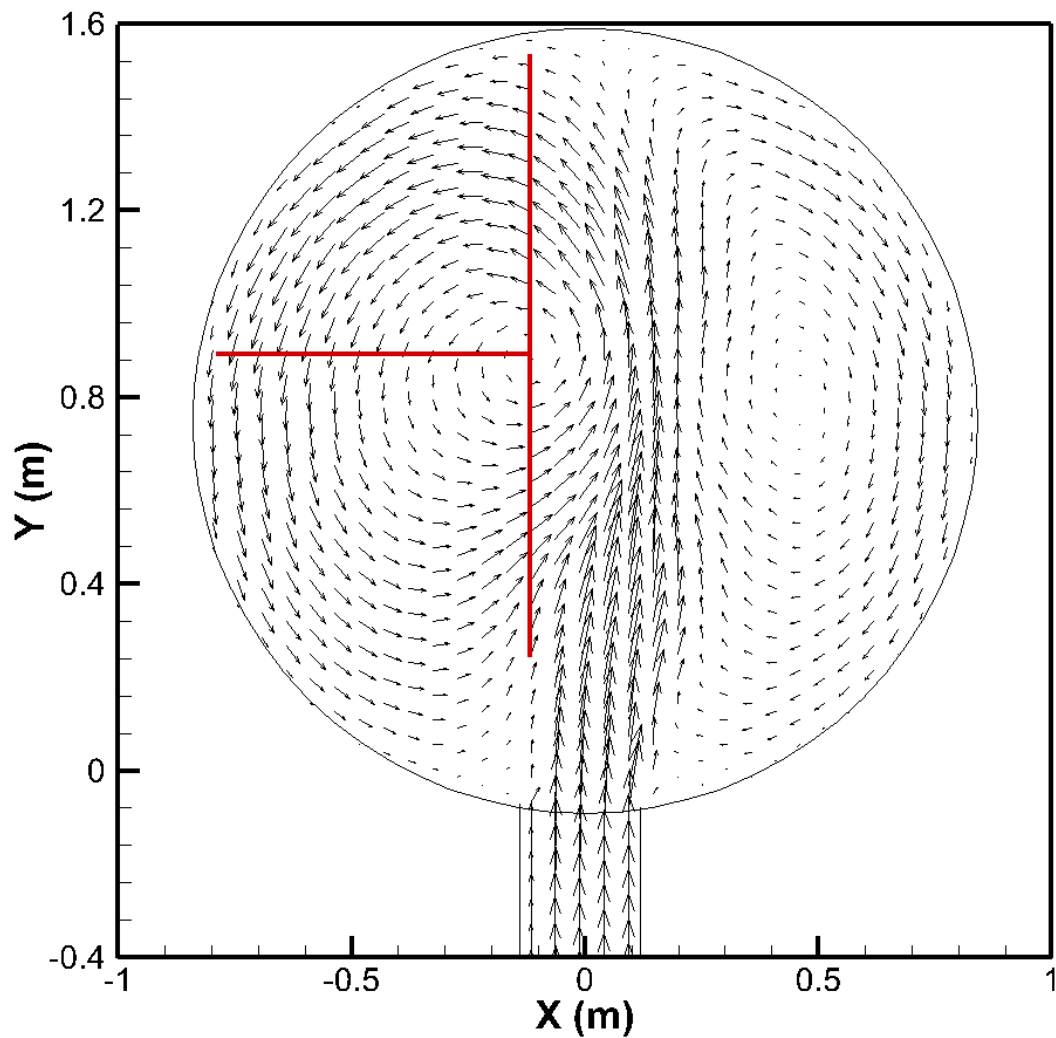
Figure 4.13 Determination of K in a cylindrical shape

Pressure levels at the outlet boundary were gradually increased with increments of 200 Pa. It was observed that, due to the changed flow geometry, the similar flow conditions develop at 8200 Pa. Thus, 8200 Pa and greater pressures were considered in the calculations. For the circular case, the required amount of outlet pressure for achieving submergence similar to original design is greater, due to the smaller head losses in the intake pond. Furthermore, circulation levels were found smaller than the original case.

The critical K value is the same as before. However, the Froude number at which the critical K is calculated is increased to 0.44.
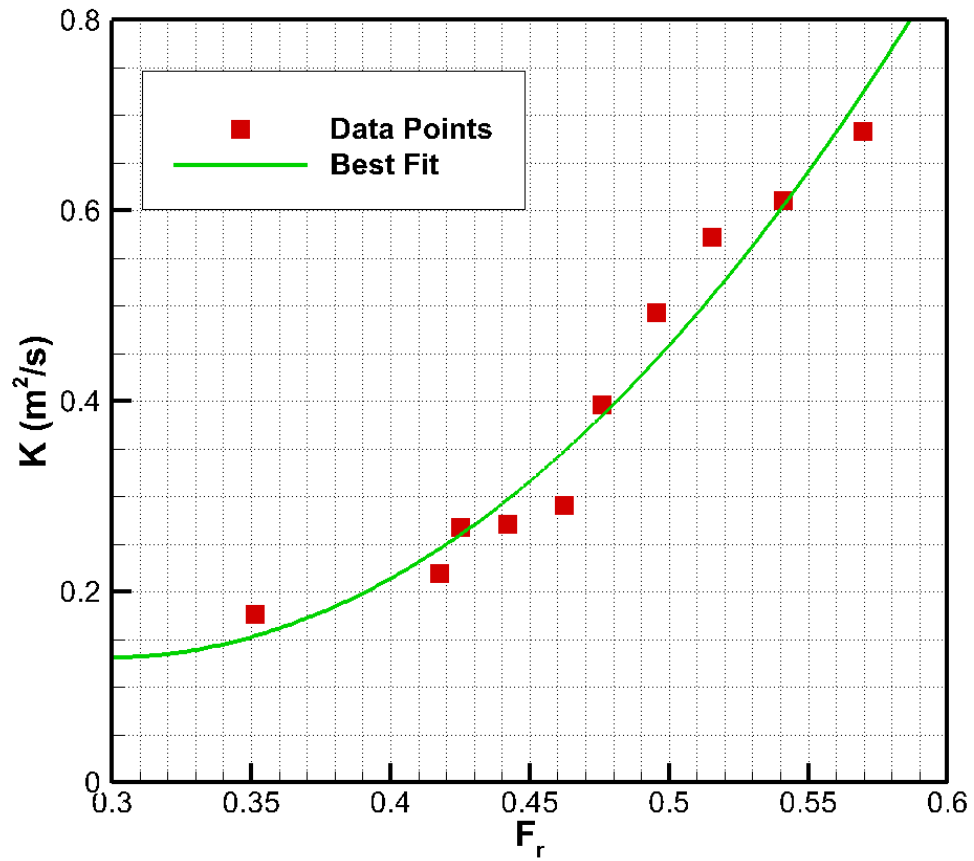
Figure 4.14. Computed vortex strengths for the cylindrical pool.

Table 4.2 Numerical data for cylindrical case with design discharge

P_{out} (Pa)	K (m²/s)	s (m)	F_r
8200	0.683	0.147	0.570
8400	0.609	0.163	0.541
8600	0.571	0.180	0.516
8800	0.492	0.195	0.496
9000	0.395	0.211	0.476
9200	0.289	0.224	0.462
9400	0.270	0.245	0.442
9600	0.266	0.264	0.425
9800	0.219	0.274	0.418

57
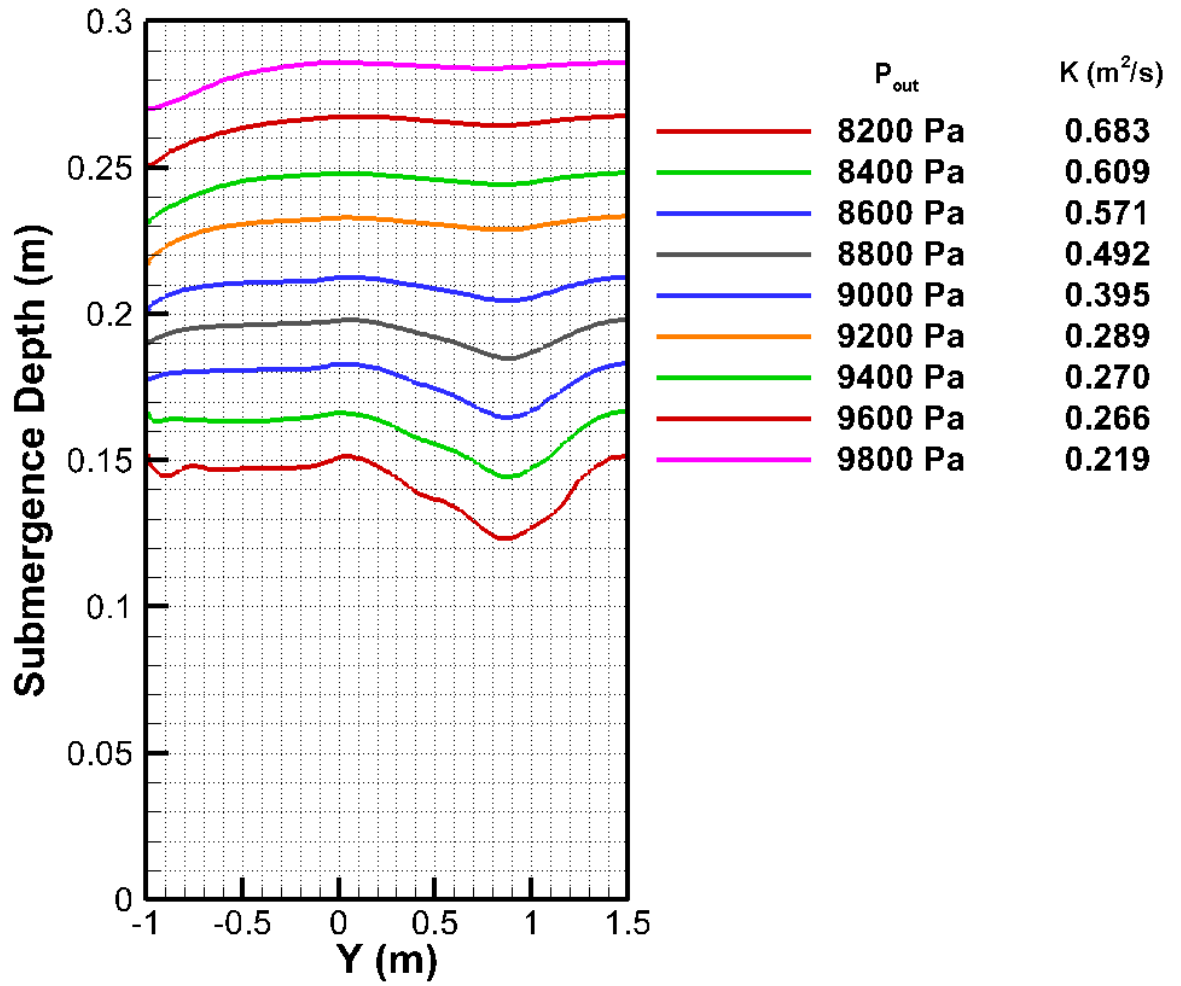
Figure 4.15 Free surface profiles in the cylindrical pool.

CHAPTER 5

CONCLUSIONS AND RECOMMENDATIONS

Vortex formation in the power intakes of hydroelectric power plants is an occasionally encountered problem which may lead to many undesired consequences. Intake vortices may even cause suspension of system operation. Prediction of vortex formation in power intakes can be tricky, since each case can be considered as unique due to the specific geometry and flow conditions. Developing solutions for vortex formation may increase construction cost and usually requires hydraulic modeling. Furthermore, in the model studies certain difficulties should be overcome, such as scale effects and fixing appropriate boundary conditions.

To solve the problem of vortex formation in intakes, CFD tools can be used beforehand, to predict possible vortex development in the flow domain. On the other hand, reliability of the CFD solutions has to be examined thoroughly to prove their validity for each specific flow configuration. This study is intended to serve for this purpose.

The numerical solutions obtained from Flow 3D revealed that CFD applications can successfully reproduce vortex motion within the flow domain. Results are satisfactorily accurate confirming experimental findings from the physical models. However, one should be very cautious while setting the boundary conditions in the computational model. Since the physical model observations

were available in the present study, it was possible to verify the outcome of the applied boundary conditions.

In velocity measurement, more accurate results were obtained for high discharge levels. In low discharges, velocity magnitudes were small and therefore, ADV measurement errors became more pronounced. Furthermore, velocity measurements near the vortex core were challenging due to three-dimensionality of flow in this zone and oscillations of the free surface in horizontal and vertical planes.

The major findings of the experimental and numerical studies are listed below:

1) In the experimental study of the head pond of Adacami project, an air entraining vortex was identified for the design discharge. To avoid vortices, it was not possible to increase the submergence due to topographic conditions. Therefore, anti-vortex structures were designed to prevent circulation and vortex formation.

2) Commercial CFD code Flow 3D was used to simulate the vortex motion in the model scale. Computational domain included the complete head pond, a part of the conveyance tunnel and the inlet transition from the head pond to the vertical penstock entrance. Natural boundary condition at the inflow and pressure boundary condition at the outflow section were found to be successful in reproducing the flow field with the vortex.

3) Vortex strength as defined in potential theory was calculated from measured and computed velocity fields. Experimental and computational values of the vortex strength were satisfactorily close to each other with nearly 15% error at high flow rates. The major source of the error is assumed to come from the measured velocity field. Vortex strengths calculated for variable submergence were shown as a function of the submergence Froude number.

4) Flow simulations were repeated with an idealized symmetrical square pool domain to study the vortex formation. However, it was not possible to reproduce an air entraining vortex in the flow field. Various boundary conditions and asymmetrical forcing were tried but all simulations failed to detect an air entraining vortex. Since there is no experimental data for this intake pool geometry no conclusion for the existence of vortices could be made.

5) Flow simulations were repeated with an idealized circular pool domain to study the vortex formation. The resulting vortices were very similar to the original design case. Vortex strength calculations were repeated and presented as function of the Froude number. The critical vortex strength for both circular and original geometries are almost equal (K=0.3 m^2/s) but the Froude numbers at which critical vortex strengths were obtained are different that are 0.44 and 0.38 respectively.

6) In conclusion, the Flow 3D code may be used to describe vortices at intakes. However, there is the risk of not identifying a vortex for certain pool geometries.

7) This study may be extended to obtain dimensionless representations for the vortex strength to be able to discuss model-prototype relations.

REFERENCES

Anwar, H.O. (1965), *Flow in a Free Vortex*. Water Power 1965(4), 153-161.

Anwar, H.O. (1966), *Formation of a Weak Vortex.* Journal of Hydraulic Research 4(1), 1-16.

Anwar, H.O. (1967), *Vortices at Low Head Intakes*. Water Power 1967(11), 455-457.

Anwar, H.O. (1968), *Prevention of Vortices at Intakes*. Water Power 1968(10), 393-401.

Aydın, İ. and Köken M.(2011), Report about Adacami Dam Power Intake

Blaisdell, F.W. and Donnelly, C.A. (1958), *Hydraulics of Closed Conduit Spillways: Part X, The Hood Inlet*. Technical Paper 20, Series B, Agricultural Research Service, St. Anthony Falls Hydraulic Laboratory, Minneapolis, Minnesota.

Brocard, D.N., Beauchamp, C.H., Hecker, G.E., (1982), *Analytic Predictions of Circulation and Vortices at Intakes*. Electrical Power Research Institute, Research Project 1199-8, Final Report.

Computational Fluid Dynamics Software - Flow 3D from Flow Science, CFD. www.flow3d.com last visited on 23/05/2012.

Daggett, L.L. and Keulegan, G.H. (1974), *Similitude in Free-Surface Vortex Formations*. Journal of Hydraulic Engineering, ASCE, HY11, 1565-1581.

Durgin, W.W. and Hecker, G.E. (1978), *The Modeling of Vortices in Intake Structures*. Proc IAHR-ASME-ASCE Joint Symposium on Design and Operation of Fluid Machinery, CSU Fort Collins, June 1978 vols I and III.

Einstein, H.A. and Li, H.L. (1955), *Steady Vortex in a Real Fluid.* La Houllie Blanche, 483-496.

Flow 3D Lecture Notes, Hydraulics Training Class.

Granger, R. (1966), *Steady Three Dimensional Vortex Flow.* Journal of Fluid Mechanics, 25(3), 557-576.

Goring, D.G, Nikola, V.I. (2002), *Despiking Acoustic Doppler Velocimeter Data.* Journal of Hydraulic Engineering, Vol. 128, No. 1, 117-126.

Guidelines for Design of Intakes For Hydraulic Plants (1995), Comitee on Hydropower Intakes of the Energy Division of the American Society of Civil Engineers, New York.

Gulliver, J.S. and Rindels, A.J. (1987), *Weak Vortices at Vertical Intakes.* Journal of Hydraulic Engineering, ASCE, HY9, 1101-1116.

Hirt, C.W. and Nichols, B.D. (1981), *Volume of Fluid (VOF) Method for the Dynamics of Free Boundaries.* Journal of Computational Physics 39, 201.

Hite, J.E. and Mih, W.C. (1994), *Velocity of Air-Core Vortices at Hydraulic Intakes.* Journal of Hydraulic Engineering, ASCE, HY3, 284-297.

Lewellen, W.S. (1962), *A Solution For Three-Dimensional Vortex Flows with Strong Circulation.* Journal of Fluid Mechanics, 420-432.

Knauss, J. (1987), *Swirling Flow Problems at Intakes.* A.A Balkema, Rotterdam.

Nichols, B.D and Hirt, C.W. (1975), *Methods for Calculating Multi-Dimensional Transient Free Surface Flows Past Bodies.* Proc. First Intern. Conf. Num. Ship. Hydrodynamics, Gaithersburg, ML, Oct. 20-23.

Odgaard, A.J. (1986), *Free-Surface Air Core Vortex.* Journal of Hydraulic Engineering, ASCE, HY7, 610-620.

Padmanabhan, M. and Hecker, G.E. (1984), *Scale Effects in Pump Sump Models*. Journal of Hydraulic Engineering, ASCE, 110, HY11, 1540-1556.

Prosser, M.J. (1977), *The Hydraulic Design of Pump Sumps and Intakes*. British Hydromechanics Research Association/Construction Industry Research and Information Association.

Potter, M.C., Wiggert, D.C., Hondzo, M., Shih T. I-P., (2002), *Mechanics of Fluids 3rd Edition*. Brooks/Cole, USA.

Rajendran, V.P., Constantinescu, G.S., Patel V.C. (1998), *Experiments on Flow in a Model Water-Pump Intake Sump to Validate a Numerical Model*. Proceedings of FEDSM'98, 1998 ASME Fluids Engineering Division Summer Meeting June 21-25, Washington, DC

Toyokura, T. and Akaike S., (1970), *Vortex Phenomena in a Water Tank*. Bull JSME, 13 (57), 373-381.

Yıldırım, N. (2004), *Critical Submergence for a Rectangular Intake*. Journal of Engineering Mechanics, Vol. 130, No. 10, 1195-1210.

Yıldırım N. and Kocabaş F. (1995), *Critical Submergence for Intakes at Open channel flow*. Journal of Hydraulic Engineering, ASCE, 121, HY12, 900-905.

Yıldırım, N., Kocabaş, F. and Gülcan, S.C. (2000), *Flow-Boundary Effects on Critical Submergence of Intake Pipe*. Journal of Hydraulic Engineering., ASCE, 126,HY4, 288-297.